PNNL-23777

Coal-Derived Warm Syngas Purification and CO_2 Capture-Assisted Methane Production

Final Report

October 2014

RA Dagle
XS Li
KA Spies
JE Rainbolt
B Braunberger
DL King
R Xing
Y Zhu
L Li

Prepared for the U.S. Department of Energy
under Contract DE-AC05-76RL01830

DISCLAIMER

PACIFIC NORTHWEST NATIONAL LABORATORY
operated by
BATTELLE
for the
UNITED STATES DEPARTMENT OF ENERGY
under Contract DE-AC05-76RL01830

Printed in the United States of America

Available to DOE and DOE contractors from the
Office of Scientific and Technical Information,
P.O. Box 62, Oak Ridge, TN 37831-0062;
ph: (865) 576-8401
fax: (865) 576-5728
email: reports@adonis.osti.gov

Available to the public from the National Technical Information Service
5301 Shawnee Rd., Alexandria, VA 22312
ph: (800) 553-NTIS (6847)
email: orders@ntis.gov <http://www.ntis.gov/about/form.aspx>
Online ordering: http://www.ntis.gov


This document was printed on recycled paper.
(8/2010)

PNNL-23777

Coal-Derived Warm Syngas Purification and CO_2 Capture-Assisted Methane Production

Final Report

RA Dagle[1]
XS Li[1]
KA Spies[1]
JE Rainbolt[1]
B Braunberger[2]
DL King[1]
R Xing[1]
Y Zhu[1]
L Li[1]

October 2014

Prepared for
the U.S. Department of Energy
under Contract DE-AC05-76RL01830
(Work for Others Agreement No. 61137)

Pacific Northwest National Laboratory
Richland, Washington 99352

[1] Pacific Northwest National Laboratory, Richland, Washington
[2] Western Research Institute, Laramie, Wyoming

Executive Summary

Gasifier-derived synthesis gas (syngas) from coal has many applications in the area of catalytic transformation to fuels and chemicals. Raw syngas must be treated to remove a number of impurities that would otherwise poison the synthesis catalysts. Inorganic impurities include alkali salts, chloride, sulfur compounds, heavy metals, ammonia, and various phosphorus-, arsenic-, antimony-, and selenium-containing compounds. Systems comprising multiple sorbent and catalytic beds have been developed for the removal of impurities from gasified coal using a warm cleanup approach. This approach has the potential to be more economic than the currently available acid gas removal approaches and improves upon currently available processes that do not provide the level of impurity removal that is required for catalytic synthesis application. Gasification also lends itself much more readily to the capture of carbon dioxide (CO_2), which is important in the regulation and control of greenhouse gas emissions.

Carbon dioxide capture material was developed for the warm temperature range (250 to 400ºC) and in this study was demonstrated to assist in methane production from the purified syngas. Simultaneous CO_2 sorption enhances the carbon monoxide methanation reaction through relaxation of thermodynamic constraint, thus providing economic benefit rather than simply consisting of an add-on cost for carbon capture and release. Molten and pre-molten $LiNaKCO_3$ can promote magnesium oxide (MgO) and MgO-based double salts to capture CO_2 with high cycling capacity. A stable cycling CO_2 capacity up to 13 mmol/g was demonstrated. This capture material was specifically developed in this study to operate in the same temperature range and therefore integrate effectively with warm gas cleanup and methane synthesis. By combining syngas methanation, water-gas-shift, and CO_2 sorption in a single reactor, single pass yield to methane of 99% was demonstrated at 10 bar and 330^{o}C when using a 20 wt% $Ni/MgAl_2O_4$ catalyst and a molten-phase promoted MgO-based sorbent. Under model feed conditions both the sorbent and catalyst exhibited favorable stability after multiple test cycles.

Warm gas cleanup of inorganics was broken down into three major steps: removal of chloride, removal of sulfur, and removal for a multitude of trace metal contaminants. Sodium carbonate was found to optimally remove chlorides at an operating temperature of 450ºC. For sulfur removal, two regenerable ZnO beds are used for bulk hydrogen sulfide removal at 450ºC (<5 ppm sulfur) and a non-regenerable ZnO bed for H_2S polishing at 300ºC (<40 ppb sulfur). We also found that sulfur from carbonyl sulfide could be adsorbed (to levels below our detection limit of 40 ppb) in the presence of water that leads to no detectable slip of H_2S. Finally, a sorbent material composed of copper and nickel was found to be effective in removing trace metal impurities such as AsH_3 and PH_3 when operating at 300ºC.

Proof-of-concept of the integrated cleanup process was demonstrated with gasifier-generated syngas produced at the Western Research Institute using Wyoming Decker Coal. When operating with a ~1 SLPM feed, multiple inorganic contaminant removal sorbents and a tar-reforming bed was able to remove the vast majority of contaminants from the raw syngas. Employing a tar-reforming catalyst was necessary due to the tars generated from the coal gasifier used in this particular study. It is envisioned that, in a real application, a commercial scale coal gasifier operating at a higher temperature would produce a smaller or negligible amount of tar. Continuous operation of a poison-sensitive copper-based water-gas-shift catalyst located downstream from the cleanup steps resulted in successful demonstration.

Preliminary technoeconomic analysis confirmed that the warm syngas cleanup process offers potential for significant thermal efficiency compared to the significant heat loss associated with water quenching and scrubbing in the cold syngas cleanup process. However, areas of improvement are needed for this technology; specifically, the CO_2 sorbent kinetics need to be improved before commercial implementation becomes practical. Relatively high equipment cost required for the integrated synthesis and sorption bed(s) would be alleviated for systems with lower CO_2 capture requirements, such as to produce syngas instead of natural gas or hydrogen. Overall, given future material improvements, there is clear potential for economic benefit.

Acknowledgments

This work was financially supported by the State of Wyoming and was performed at Pacific Northwest National Laboratory (PNNL) and at the Western Research Institute (WRI). Some financial support was offered by the U.S. Department of Energy (DOE), Office of Fossil Energy, and PNNL internal research funds. PNNL, located in Richland, Washington, is a multi-program national laboratory operated for DOE by Battelle Memorial Institute. WRI, located in Laramie, Wyoming, is a technology development center serving private clients, industry, and government with expertise in energy, environment, and highway material. A portion of this work was done in the William R. Wiley Environmental Molecular Sciences Laboratory, which is a DOE sponsored scientific user facility located at PNNL. Finally, the authors would like to acknowledge Cary Counts of PNNL for his expert and tireless editorial reviews in support of this report.

Acronyms and Abbreviations

AGR	acid gas removal
ASU	air separation unit
BET	Brunauer-Emmett-Teller
CO_2	carbon dioxide
CO	carbon monoxide
COS	carbonyl sulfide
DOE	U.S. Department of Energy
DSC	differential scanning calorimetry
GC	gas chromatography
GHSV	gas hourly space velocity
HCl	hydrogen chloride
ICP	inductivity coupled plasma
IGCC	integrated gasification combined cycle
PM	particulate matter
PNNL	Pacific Northwest National Laboratory
PSA	pressure swing adsorption
PSW	pressure swing
sccm	standard cubic centimeters per minute
SCD	sulfur-chemiluminescence detector
SEM	scanning electron microscopy
SiC	silicon carbide
SNG	synthetic natural gas
TGA	thermogravimetric analyzer
TPB	triple phase boundary
WGS	water-gas-shift
WRI	Western Research Institute
XRD	X-ray diffraction
ZnO	zinc oxide
ZnS	zinc sulfide

Contents

Figures

Tables

1.0 Introduction

The production and use of synthesis gas (syngas) from gasified coal, biomass, or heavy hydrocarbons has been the subject of many studies. Because the raw syngas produced includes several impurity species, the end use of the syngas dictates the level of treatment of the syngas that is required. Notable among the impurity species are the sulfur-based gases hydrogen sulfide (H_2S) and carbonyl sulfide (COS), and to a much lesser extent carbon disulfide (Xiao et al. 2012). For more sulfur-tolerant industrial processes, such as integrated gasification combined cycle (IGCC) operation, sulfur is removed using a warm gas cleanup (350 to 500ºC), zinc oxide (ZnO)-based regenerable moving sorbent bed that reduces the sulfur content down to a few parts per million by volume (ppmv) (Xiao et al. 2012, King and Li 2011). However, industrial processes intolerant to sulfur include processes that use syngas to produce chemical or fuel products (e.g., methanol, synthetic natural gas [SNG], Fischer-Tropsch liquids, mixed alcohols, etc.) and for power generation with fuel cells (e.g., proton exchange membrane fuel cell or solid oxide fuel cell). Because these processes require maximum sulfur gas concentrations below 100 parts per billion by volume (ppbv), the standard commercial unit operation is chilled methanol solvent to remove sulfur species to the required low levels (Rectisol process) (Couling 2012).

While effective in removing sulfur, low-temperature desulfurization processes incur economic penalties in that the syngas is substantially cooled for purification and then reheated to synthesis temperatures for use (Couling 2012). With end uses for the syngas such as fuel or chemical synthesis, where catalytic conversions occur in the range of 200 to 350ºC, warm gas cleanup methods (300 to 450ºC) may be employed. For warm gas cleanup, ZnO-based sorbents have become the leading material because of its high sulfur affinity and high sulfur capacity, and its ability to be regenerated (Xiao et al. 2012). Zinc oxide has a theoretical sulfur capacity of 0.393 gram of sulfur per gram of ZnO, which is one of the highest capacities for metal oxides (Elseviers and Verelst 1999).

For control of greenhouse gas emissions, carbon dioxide (CO_2) should be captured. Capture of CO_2 at warm temperatures is advantageous in terms of thermal efficiency compared to cooling the gas to liquid absorbent temperatures and then reheating to the temperature of use. The subsequent water-gas-shift (WGS) reaction can be used to adjust the hydrogen/carbon monoxide (H_2/CO) ratio or for hydrogen production. By capturing CO_2 during the shift reaction, the equilibrium conversion of CO can be increased and, in addition, capturing CO_2 at this point allows more total CO_2 to be captured. Especially attractive is a combined bed that contains both CO_2 capture material and WGS catalyst. Alternatively, if SNG is the desired end product, combining CO_2 capture with CO methanation offers a similar advantage.

The objective of this study is to develop the materials for and demonstrate the successful removal of inorganic impurities and CO_2 present in gasified Wyoming-derived sub-bituminous coal. The end product for this particular study is a clean syngas feed that is converted to high purity methane. However, this approach could be applied to the cleanup of syngas useful for the synthesis of other fuels and chemicals. Our general cleanup strategy is to be able to remove the impurities in the raw syngas irrespective of whether a syngas cooling-water quench is employed. The water quench step typically removes some of the impurities in the syngas, depending on the temperature, at some loss in efficiency. We designed our cleanup system to include the possibility that no syngas cooler water quench will be employed.

In this report, we describe the materials that were developed for CO_2 and sulfur sorption, and for the removal of other impurities such as chloride, alkali, ammonia, and heavy metals (e.g., arsenic, phosphorus, antimony, selenium, mercury, etc.). Also discussed is development of the CO_2 sorption-enhanced CO methanation process, a technoeconomic analysis, and demonstration results from an entire integrated process train using actual Wyoming coal-derived syngas. Figure 1.1 is a diagram of the integrated warm gas cleanup process that was developed in this study.

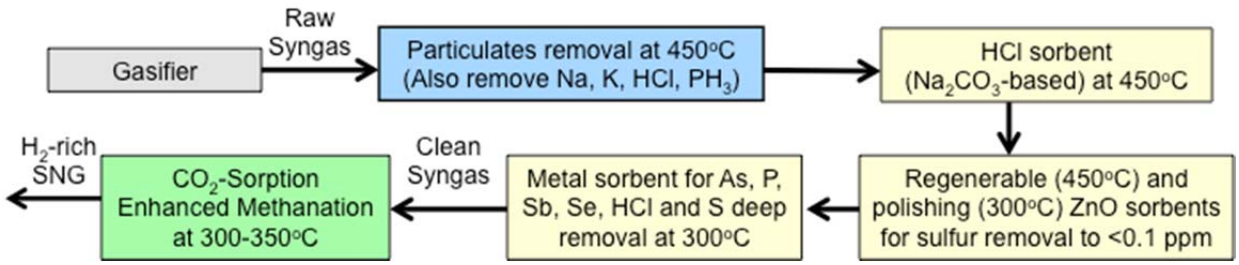

Figure 1.1. Warm Coal-Derived Syngas Cleanup Approach for Generation of SNG

It should be noted that the approach described in this study also can be generally applied to the cleanup of biomass-derived syngas. While the concentrations of impurities differ, similar processing steps could be applied. One difference pertains to the tar impurities (i.e., polycyclic aromatic hydrocarbons) typically contained in biomass-derived syngas. Several tar-removal strategies have been reported including physical (e.g., scrubbing) and catalytic (e.g., cracking, reforming) approaches (Torres et al. 2007). A tar-reforming catalyst was employed in this study for coal-derived cleanup application. A tar-reforming unit was justified because of the low operating temperature employed by the gasifier used in this study, which resulted in the production of tars. It is envisioned that a real application for coal gasification would be at a significantly higher temperature, thus resulting in minimal tar production.

2.0 Experimental Method

2.1 Adsorbent Materials Synthesis

Figure 2.1 schematically shows the procedure used to synthesize the MgO-based sorbents. Typically, MgO powder with $NaNO_3$ (>99%, ACROS Organics) or the eutectic mixture of LiNaK-CO_3 first were mixed at a desired weight ratio to form a solid mixture by ball milling. Then, 20 to 30 g of solid mixtures, 50 to 90 g of 2-propanol (Fisher Scientific), and 100 to 160 g of zirconia beads (diameter: 0.3~1 cm) were added into a 125 mL Nalgene plastic bottle. The mixture was ball milled for 48 to 72 hours at a speed of 60 rpm. The resulting slurry was dried at 25ºC in a 12 inch × 9 inch tray to allow the evaporation of 2-propanol. After drying, the thin white cake was calcined at 350to 450ºC in air for 3 hours. The resulting material was crushed and sieved to 40 to 60 mesh size. Three sorbents were evaluated, and their composition and physical properties are summarized in Table 2.1.

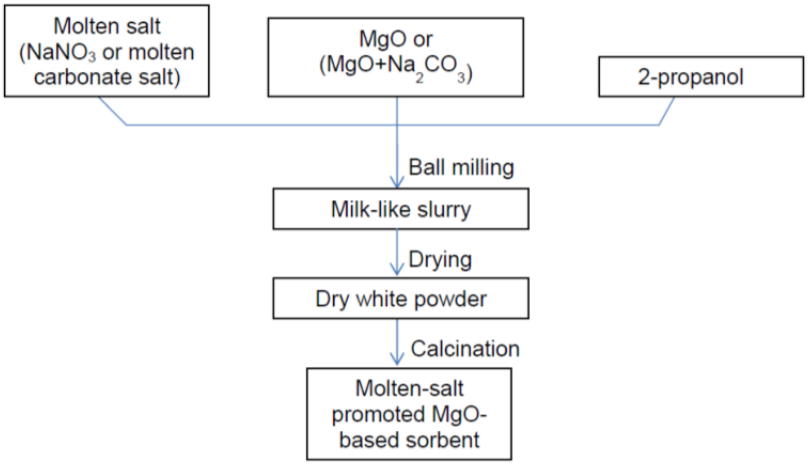

Figure 2.1. Simplified Procedure for Preparing Molten Salt Promoted MgO-Based Sorbent

Table 2.1. Summary of the Physical Properties of Fresh Sorbents Investigated in this Work

Sorbent	Composition	Calcination Temperature °C	BET Surface Area m^2/g	Pore Volume cm^3/g	MgO Crystal Size nm
-1	77 wt%MgO, 11 wt%Na_2CO_3, 12 wt%$NaNO_3$	450	31.3	0.3	10.9
-2	44 wt% MgO, 48 wt% Na_2CO_3, 4 wt% Li_2CO_3, 4wt% K_2CO_3	450	7.3	0.05	21.0
-3	80 wt% MgO, 20 wt% LiNaK-CO_3	350	36.8	0.56	7.61

A multi-contaminant sorbent consisting of copper and nickel on activated carbon was used to remove trace metals and low concentrations of sulfur. The activated carbon, KOA-13 PACO carbon, was processed to remove any trace sulfur before any metal was added. To remove the trace sulfur, the carbon material went through a nitric acid wash step and was calcined in a carbon furnace. The nitric acid wash

was performed by mixing the carbon with 4-M nitric acid on a hot stir plate at 80ºC for 6 hours. The acid was removed with repeated rinses with deionized water. After drying in an oven at 110ºC with a nitrogen (N_2) atmosphere overnight to remove leftover moisture, the material was placed in a carbon furnace where it was heated up to 1800ºC under helium for 8 hours with a 5ºC/min ramp. The final material was tested for sulfur using inductivity coupled plasma (ICP), and no sulfur was detected.

Copper and nickel were added to the carbon by wet impregnation to a desired loading of 8% nickel and 1% copper. The final sorbent was loaded in a fixed-bed reactor and reduced at 300ºC for 8 hours under 10% H_2 in N_2 prior to running.

2.2 Catalyst Synthesis

In this work, the 20wt% Ni/$MgAl_2O_4$ catalyst used for the CO methanation reaction and was prepared by incipient wetness impregnation of $MgAl_2O_4$ (Sasol Puralox 30/140) with a solution of nitrate hexahydrate (Sigma-Aldrich 99%) dissolved in acetone. After impregnation, the catalyst was dried at 110^{o}C for 8 hours and calcined in air at 350ºC for 3 hours. We used a nickel loading of 20 wt% in this work.

Supported iridium catalyst was used as the tar-reforming catalyst as described in our earlier work (Mei et al. 2013, 2014). It was prepared by incipient wetness impregnation of $MgAl_2O_4$ (Sasol Puralox 30/140). The support was calcined at 500ºC, and iridium nitrate (Sigma-Aldrich 99%) was dissolved in deionized water. After impregnation, the catalysts were dried at 110ºC for 8 hour and calcined under air at 500ºC for 3 hour. The metal loading was 5 wt% and designated as 5% Ir/$MgAl_2O_4$ and reduced at 850ºC under 10% H_2 (balance N_2) for 2 hours prior to operation.

2.3 Materials Characterization

The Brunauer, Emmett, and Teller (BET) surface areas were measured by N_2 adsorption at 77 K with an automatic gas sorption system (Quantachrome Autosorb-6B). The samples were degassed under vacuum at 150ºC for 8 to 16 hours before the adsorption measurements. The surface area was determined using the five-point BET method, and the Barrett-Joyner-Halenda method was used for the pore volume determination. X-ray diffraction (XRD) patterns were recorded using a Rigaku diffractometer with a copper anode (wavelength = 0.15405 nm) and a scanning rate of 0.008^o per second between $2\theta = 10^o$ and 80^o. The diffraction patterns were analyzed using PDXL-2 software and the Powder Diffraction File database. Particle sizes of the samples were determined from the XRD patterns using the Debye-Sherrer relation ($d = 0.89\lambda/B\cos\theta$, where λ is the wavelength of copper Kα radiation, B is the calibrated half-width of the peak in radians, and θ is the diffraction angle of a crystal face). The particle sizes were determined from the peaks located at $2\theta = 52^o$ and 43^o, respectively, for nickel and MgO. Scanning electron microscopy (SEM) measurements were conducted with an FEI Quanta 3D FEG microscope. The SEM sample preparation includes mounting powder samples onto carbon discs, followed by platinum coating under a current of 15 mA for 180 seconds.

2.4 Sorbent Performance Measurements

Multi-cycle CO_2 absorption and desorption performance of sorbents was first tested with a thermogravimetric analyzer (TGA, Netzsch Thermal Analysis, STA 409 cell) at ambient pressure using a temperature-pressure combined swing. The weight of the sorbent sample for each test was ~20 mg. The temperature-pressure combined swing was conducted by exposing the sample to alternating 100% CO_2 for 60 to 99 minutes and then CO_2 release in N_2 or air flow during ramping to and holding at 385 to 450ºC for 60 to 81 minutes. The breakthrough performance of the sorbents was tested in a fixed-bed apparatus using a 9 mm inner-diameter, fixed-bed alumina reactor connected to an Agilent Micro-GC equipped with a Molsieve and a Poraplot U column. Carbonation was carried out at a temperature of between 300 and 400ºC depending on the sorbent by flowing a gas stream containing 60% CO_2 and 40% N_2. Decarbonation was performed at a temperature between 390 and 450ºC depending on the sorbent under 200 sccm N_2 or air for 1 hour. CO_2 sorption capacity is defined as the amount of CO_2 absorbed (CO_2 in mmol) per gram of sorbent.

2.5 Catalyst Reactivity Measurements

Reactivity measurements of syngas methanation reaction in the absence of sorbent were performed in a 9 mm inner-diameter, fixed-bed alumina reactor at ambient pressure. The 20 wt% $Ni/MgAl_2O_4$ catalyst diluted with silicon carbide (SiC) (5:1 weight ratio of SiC-to-catalyst) was loaded between two layers of quartz wool inside the reactor. The SiC was added to keep the catalyst bed isothermal. Two K-type thermocouples were placed into the reactor for the measurement of inlet and catalyst bed temperatures. Prior to the test, the catalyst was reduced at 850ºC using a 5% H_2/N_2 gas mixture for 3 hours. The catalysts were tested with a gas stream containing 40% H_2, 32% CO, 22% CO_2, 3% CH_4, and 3% N_2 or 34% H_2, 27.2% CO, 18.7% CO_2, 2.55% CH_4, 2.55% N_2, and 15% H_2O. Nitrogen was used as an internal reference.

2.6 Integrated-Bed Performance Measurements

At ambient pressure conditions, most of the sorption-enhanced methanation integrated-bed tests were performed in a 9 mm inner-diameter, fixed-bed alumina reactor. For high pressure tests, the integration tests were carried out in a stainless-steel reactor. Two modes of operation were employed: sequential bed and mixed bed. For the sequential-bed mode, the methanation catalyst was not mixed with the sorbent, but the catalyst bed and the sorbent bed were loaded into the reactor sequentially with 1-inch-thick quartz wool in between. This operation mode is used only for Sorbent-1, which contained $NaNO_3$ (melting point 309ºC). For the mixed-bed mode, the catalyst and the sorbent are mixed to form a single bed. In this mode, the integrated tests were performed using 0.3 g catalyst, 1.7 g diluent of silicon/carbon, and 5 g of Sorbent-2. Multiple cycles of carbonation–decarbonation were conducted in each case. Carbonation was conducted at 300 to 400ºC under syngas methanation reaction conditions. Decarbonation was carried out at 390 to 450ºC by flowing 200 sccm of N_2 for 1 hour. All feed gases were introduced into the system using MKS Mass Flow controllers. If needed, water was introduced using a syringe pump through $^1/_{16}$-inch stainless-steel tubing into a vaporizer where the temperature was set at 250ºC for all runs.

It should be noted that the CH_4 and CO_2 selectivities were calculated based on the gas phase composition only and do not include the solids products. This selectivity definition was applied for CO methanation experiments that were performed both in the absence or presence of CO_2 sorbent. To avoid confusion throughout the text selectivities are explicitly described as "gas phase selectivities" (e.g., gas phase CH_4 selectivity).

2.7 Warm Sulfur Sorption Experiments

The two ZnO sorbents used in this study, G-72D and G-72E, were obtained from Süd Chemie. The sorbent material was meshed to a particle size of 177 to 250 μm and placed inside a quartz tube reactor without further processing or pretreatment. The sorbent was held in place by quartz wool, which also served to mix the reactant gases. The carrier gases were introduced dry and humidified by a microchannel vaporizer to the desired water content. The gas stream was analyzed for sulfur by a sulfur-chemiluminescence detector (SCD) attached to a gas chromatograph. The SCD detector has a detection limit of less than 50 ppbv sulfur.

2.8 Equilibrium Calculations

The concentrations of gaseous components at thermodynamic equilibrium were determined by Gibbs free energy minimization using the ChemCAD software package. Because of the limitation of ChemCAD, only the system in the absence of sorbent was considered in this work where reactions 4.1 and 4.2 were used. CO conversion and gas product selectivity were calculated as a function of temperature and pressure in the absence or presence of water in the feed syngas.

3.0 Double-Salt Adsorbents for Carbon Dioxide Removal

3.1 Introduction

To capture CO_2 by chemisorption in the warm temperature range (250 to 400ºC) MgO-based absorbents are the most appropriate. However, the reaction between MgO and CO_2, although thermodynamically favorable, is kinetically slow. Addition of a nitrate salt, such as $NaNO_3$, which melts at the temperatures of absorption and desorption, facilitates the conversion of MgO to $MgCO_3$ (Zhang, et al. 2013, 2014). In a similar way, it assists in the capture and release of CO_2 by double salts such as $MgO\text{-}Na_2CO_3$ or $MgO\text{-}CaCO_3$. Preliminary tests indicate that $NaNO_3$ promoted MgO or double salts suffer from some difficulties in fixed-bed operation. The combination of strong oxidizing power and rapid migration of the molten-phase results in loss of molten salt to the walls of the reactor and corrosion of the metallic surfaces, including to some extent even monel and Hastelloy C. Depleting the molten salt also reduces the effectiveness of the CO_2 capture material. This molten phase would undoubtedly migrate onto the surface of any co-mixed WGS catalyst in fixed-bed operation, leading to oxidation and possibly poisoning of the surface.

We have identified a low melting eutectic material composed of $Li_2CO_3\text{-}Na_2CO_3\text{-}K_2CO_3$ that is non-oxidizing and non-corroding and has a melting point around 397ºC (Volkova 1958). This molten eutectic operates nearly as well as $NaNO_3$. To address the migration/wetting behavior, we have discovered and applied a phenomenon that has been only scarcely reported—pre-melting behavior. Although not fully understood, this behavior is associated with formation of a thin film of molten salt at the salt surface that can activate the MgO-based absorbent surface at the point of contact but not migrate (Wettlaufer and Worster 2006).[1] By proper control of operating temperature, we have been able to absorb and desorb CO_2 from these materials while avoiding any molten-phase formation, migration, or degradation. In this chapter, we briefly describe studies focused on the synthesis, characterization, and performance of these materials. Successful testing of these materials in mixed-bed catalytic operation is reported in Chapter 4.

3.2 Results

Figure 3.1 shows the TGA measurement results of 350ºC calcined MgO and 20% $LiNaKCO_3$@MgO. In the TGA measurements, the samples were heated in 100% CO_2 at ambient pressure at a heating rate of 5ºC/min. It shows a rapid conversion of ~60% of MgO to $MgCO_3$ as compared to almost no MgO conversion in the absence of $LiNaKCO_3$. An absorption rate of 4 to 5 mmol/g/min was observed at 360 to 370ºC. The results indicate that the presence of $LiNaKCO_3$ significantly improves the ability of MgO to capture CO_2.

[1] http://en.wikipedia.org/wiki/Premelting#References

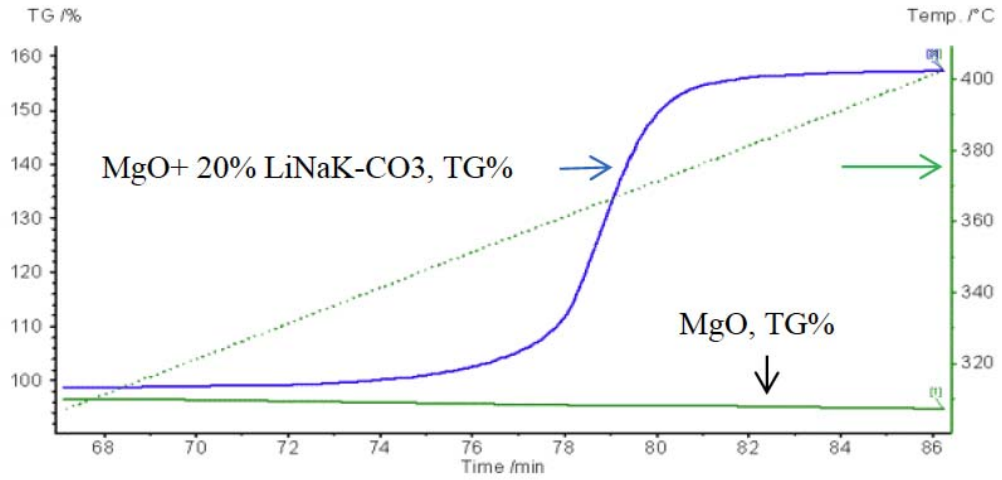

Figure 3.1. TGA Results of CO_2 Absorption on MgO and 20% $LiNaKCO_3$@MgO

Figure 3.2 shows the cyclic CO_2 absorption/desorption profile of 350ºC calcined 20% $LiNaKCO_3$@MgO sample through temperature-pressure combined swing measured in TGA. The absorption was conducted in 100% CO_2 at 360ºC, while desorption was performed in N_2 at 390 to 395ºC. High stable capacity (13 mmol/g) was achieved.

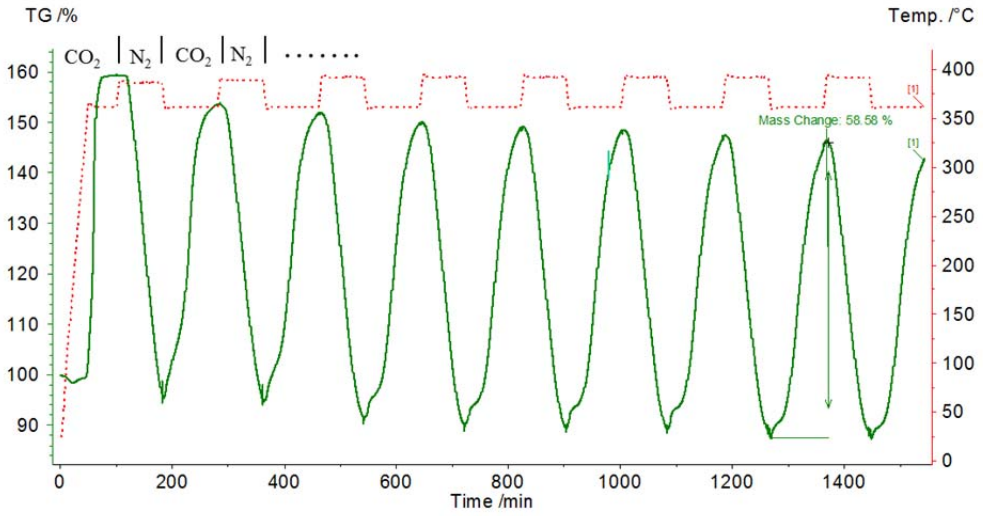

Figure 3.2. Cyclic CO_2 Absorption Test of 20%$LiNaKCO_3$@MgO through Temperature-Pressure Combined Swing

Figure 3.3 shows SEM images of 350ºC calcined 20% LiNaKCO3@MgO sample before (Figure 3.3a) and after (Figure 3.3b) CO_2 absorption. The as-prepared 20% $LiNaKCO_3$@MgO sample shows about 0.2 μm particles with rough surfaces. The formed $MgCO_3$ displays a smooth surface with a larger particle size.

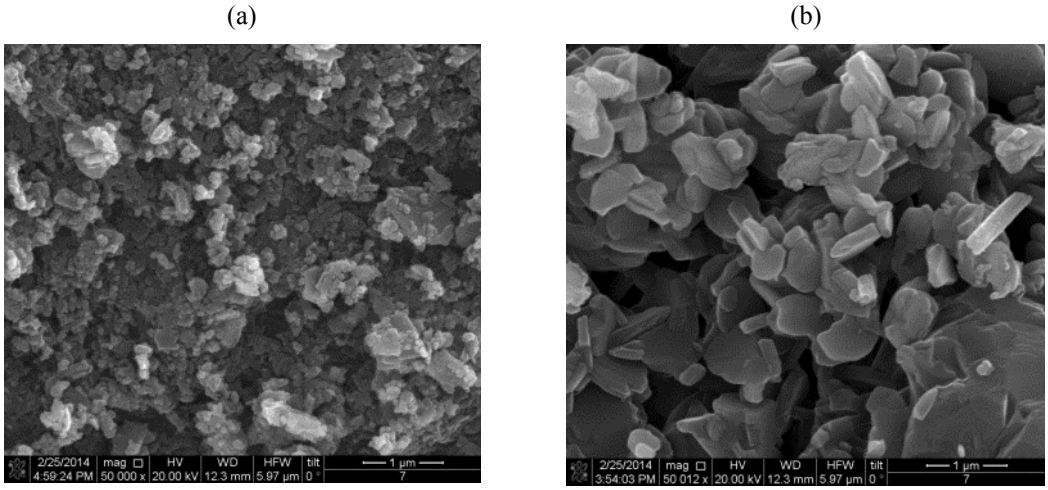

Figure 3.3. SEM Images of 350ºC Calcined 20% $LiNaKCO_3$@MgO Sample before (a) and after (b) CO_2 Absorption

We studied the effect of the $LiNaKCO_3$ concentration on the CO_2 absorption rate of MgO absorbents. Figure 3.4 shows the average rate along with the surface areas. A low absorption rate (<0.06 mmol/g/min) appears at low $LiNaKCO_3$ concentrations (below 10 wt%) and the highest rate (~2.5 mmol/g/min) is achieved at 20% $LiNaKCO_3$, then decreases to 0.7mmol/g/min as the concentration of $LiNaKCO_3$ increases to 60 wt%. The optimized $LiNaKCO_3$ concentration is 20%.

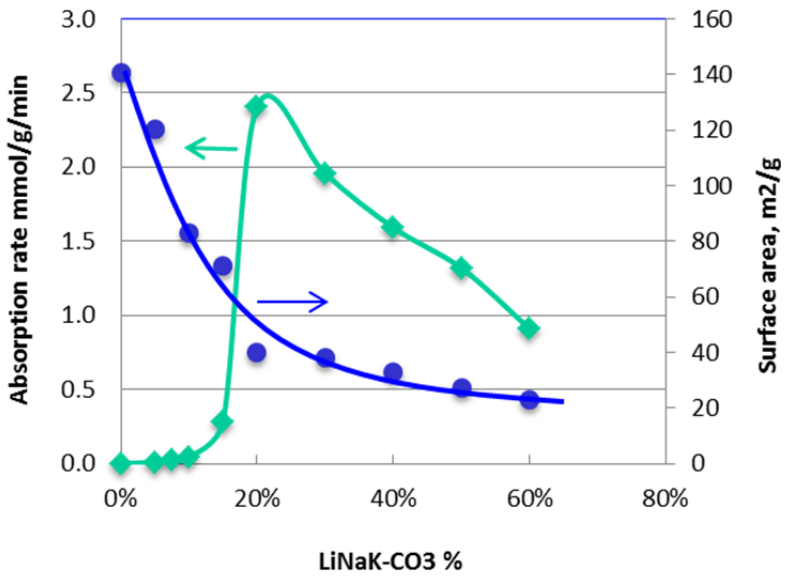

Figure 3.4. Absorption Performance and BET Surface Area of 350ºC Calcined $LiNaKCO_3$@MgO as a Function of $LiNaKCO_3$ Concentration

When its surface is completely covered by LiNaKCO3, MgO loses its ability to capture CO_2, indicating that retention of some available MgO surface is crucial to capturing gaseous CO_2. In our previous study (Zhang et al. 2014), we reported that triple phase boundaries (TPB) created by the solid MgO, molten $NaNO_3$, and gaseous CO_2 are required for MgO to capture CO_2. Figure 3.5 illustrates the

TPB mechanism (Zhang et al. 2014). At temperature of 330 to 375ºC, $NaNO_3$(melting point 308ºC) melts and partially wets the MgO surfaces; some MgO dissolves into the molten $NaNO_3$ as solvated ionic pairs ($[Mg^{2+}\cdots O^{2-}]$) and establishes a dissolution/precipitation equilibrium; gaseous CO_2 weakly adsorbs on the bare MgO surface, and migrates to the gas-liquid-solid TPB. The adsorbed CO_2 then reacts with the $[Mg^{2+}\cdots O^{2-}]$ ionic pairs to form a $[Mg^{2+}\cdots CO_3^{2-}]$ ionic pairs that precipitate as solid $MgCO_3$ when saturation is reached.

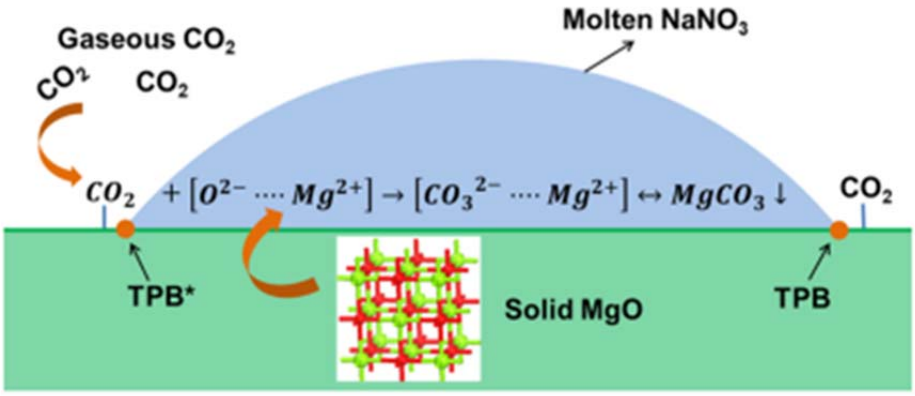

Figure 3.5. Illustrative Diagram for the Phase Transfer Catalysis of CO_2 Absorption on MgO with Molten $NaNO_3$ (TPB* = triple phase boundary) (Zhang et al. 2014)

3.3 Conclusions

Molten and pre-molten $LiNaKCO_3$ can promote MgO and MgO-based double salts to capture CO_2 with a high cycling capacity. Molten carbonate also can promote the decomposition of $MgCO_3$. A stable cycling CO_2 capacity of up to 13 mmol/g was achieved. Gas-solid-liquid TPBs are required for LiNaK CO_3@MgO to effectively capture CO_2. By adjusting the composition of the absorbent, a series of absorbents that can be used for different applications were developed.

4.0 Carbon Dioxide Sorption-Assisted Methanation

4.1 Introduction

Production of SNG via a thermo-chemical process includes three main steps: 1) gasification of the coal/biomass, 2) gas cleaning and conditioning, and 3) methanation. Gas conditioning refers to a process (e.g., steam reforming, WGS, etc.) in which components of the gases produced from the gasification are converted to a composition that is suitable for the methanation reactions. The production gas consists of H_2, CO, CO_2, H_2O, CH_4, and some higher hydrocarbons like tar and impurities such as sulfur, chlorine, and metal species. After gas cleaning, the production gas can be converted into CH_4-rich gases mainly by the following reversible methanation reaction:

$$CO + 3H_2 \leftrightarrow CH_4 + H_2O \qquad \Delta H^0_{298K} = -206 KJ/mol \tag{4.1}$$

Reaction 4.1 is thermodynamically favored at a low temperature but kinetically favored at a high temperature. In addition, a high pressure favors the shift of the reaction equilibrium to the right side, thus increasing the CO conversion and CH_4 recovery. As a result, conversion of syngas to SNG typically is operated at moderate temperatures (275 to 325ºC) and an elevated pressure to avoid the thermodynamic barrier and to ensure high CH_4 yields and a reasonably fast reaction rate (Kopyscinski et al. 2010). Because water usually is present in the syngas stream and is also a product of methanation reactions, the WGS reaction occurs as well:

$$CO + H_2O \leftrightarrow CO_2 + H_2 \qquad \Delta H^0_{298K} = -41 KJ/mol \tag{4.2}$$

Reactions 4.1 and 4.2) are both exothermic, which suggests that a heat of reaction has to be considered for SNG production. Actually, the outlet temperature of the reactor usually is 150 to 350ºC higher than the inlet temperature in many existing commercial processes (Kopyscinski et al. 2010).

Reactions 4.1 and 4.2 are reversible. According to thermodynamics, the presence of CO_2 is not in favor of the CH_4 formation because it tends to shift the reactions to the left side, thus decreasing the CH_4 yield and the CO conversion. Carbon dioxide produced in the methanation and WGS reactions should be immediately removed to enhance CH_4 yield. Integration of the syngas methanation reaction with in situ CO_2 capture has received increasing attention in an effort to ease the thermodynamic constraints on CO conversion and the resulting CH_4 yield, to mitigate CO_2 emissions into the atmosphere, and to increase the overall efficiency of the process (Lebarbier et al. 2014).

Recently, Liu and Qin (2012) disclosed a conceptual system for producing CH_4-rich gases from syngas. The system includes a reactor and at least one sorbent regenerator, where the reactor retains methanation catalyst while allowing sorbent for CO_2 and sulfide gas (H_2S and COS) to pass through the reactor. Carbon dioxide and sulfide gas are removed simultaneously from the methanation reaction system by the sorbent. The saturated sorbent can be regenerated in the generator and recycled into the system. Although the concept works, there are no real experimental data supporting it. Lebarbier et al. (2014) recently reported a system, combining CO methanation, WGS, and CO_2 capture that demonstrated enhanced CH_4 yield from 22% to ~90%. In that case, the CaO-based sorbent was used for CO_2 capture.

The temperatures required for the carbonation and decarbonation cycles were high (i.e., 600ºC and 800ºC, respectively).

It may be more desirable to operate the integration bed at a lower temperature such as 300 to 400ºC. Thus far, however, no CO_2 capture technology has been developed for practical CO_2 separation from syngas in this lower temperature range because of the limitations of existing CO_2-capture materials. As described in the previous section, we have developed a series of alkali nitrate-promoted MgO-based sorbents that show simultaneous high CO_2 sorption capacity (>10 mmol/g) and high absorption/desorption kinetics in the temperature range of 300 to 400ºC (Zhang et al. 2013, 2014). For CO_2 sorption using MgO-based sorbents, the following reversible chemical reactions exist:

$$CO_2(g) + MgO(s) \rightarrow MgCO_3(s) \quad \Delta H^0_{298K} = -118KJ/mol \quad \text{carbonation} \quad (4.3)$$

$$MgCO_3(s) \rightarrow CO_2(g) + MgO(g) \quad \text{decarbonation} \quad (4.4)$$

In the presence of Na_2CO_3, the double salt $Na_2Mg(CO_3)_2$ is formed, and the following chemical reactions occur:

$$MgO(s) + Na_2CO_3(s) + CO_2(g) \rightarrow Na_2Mg(CO_3)_2(s)$$

$$\Delta H^0_{298K} = -130KJ/mol \quad \text{carbonation} \quad (4.5)$$

$$Na_2Mg(CO_3)_2(s) \rightarrow MgO(s) + Na_2CO_3(s) + CO_2(g) \quad \text{decarbonation} \quad (4.6)$$

The goal of this study was to determine the feasibility of integrating syngas methanation with CO_2 capture into one single reactor to produce methane at high yields in the 300 to 400ºC temperature range. Figure 4.1 illustrates the simplified process flow diagram for the production of CH_4-rich gases from warm syngas derived from the coal/biomass thermal gasification. In our approach, the warm syngas after gas cleaning is sent to a reactor that combines a methanation catalyst and a sorbent capable of absorbing CO_2. Through this integration the two processes, high yields of CH_4 (>90%) are produced in the 300 to 400ºC operating temperature range. The CH_4-rich gases can be further upgraded to make fuels, and the captured CO_2 will be processed for further use or for sequestration to reduce CO_2 release to the environment.

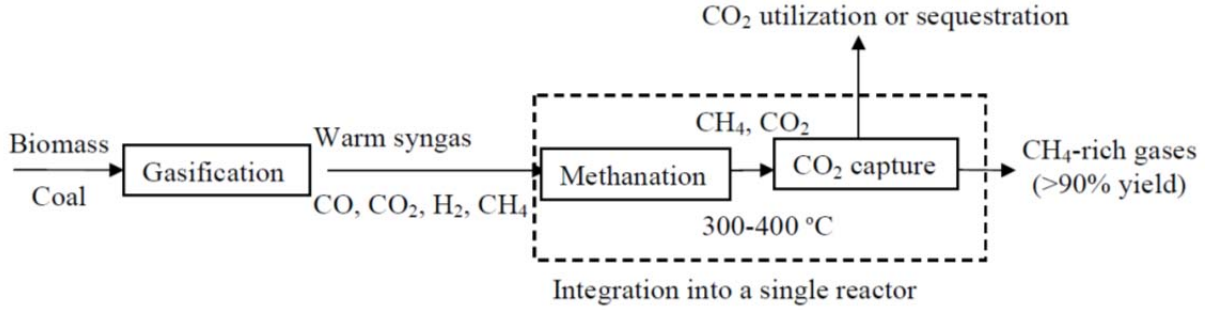

Figure 4.1. Simplified Process Flow Diagram for the Production of CH_4-Rich Gases from Warm Syngas by Integrating the Methanation Reaction with CO_2 Capture in a Single Reactor

In this study, the 20 wt% Ni/$MgAl_2O_4$ catalyst was selected as the methanation catalyst because of its high activity and favorable stability (Lebarbier et al. 2014). MgO and/or MgO-based double salt were selected as the sorbent. First, we performed the thermodynamic calculation of syngas methanation in the

absence of sorbent to predict the equilibrium CH_4 yield without CO_2 sorption. The performance of MgO-based absorbents was evaluated for CO_2 sorption in the 300 to 400°C temperature range using both TGA and fixed-bed sorption breakthrough tests. Integration of syngas methanation and CO_2 capture was demonstrated in a fixed-bed reactor using a gas mixture containing 40% H_2, 32% CO, 3% N_2, 3% CH_4, and 3% N_2 or 34% H_2, 27.2% CO, 18.7% CO_2, 2.55% CH_4, 2.55% N_2, and 15% H_2O, which simulates the gas composition of syngas produced from the gasifier at the Western Research Institute. It should be mentioned that the feed gas had a H_2/CO ratio of ~1:1, which actually is comparable to many gasifier syngas compositions. Depending on the type of molten salts used, the integrated tests were conducted in either a sequential-bed reactor or a mixed-bed reactor. Through the integrated test, we were interested in elucidating the role of CO_2 sorbent in methane production—in particular, its effect on the activity and stability of methanation catalyst. Also, we wanted to understand the effect of key process parameters such as temperature, pressure, and the addition of water to the syngas on the integration performance; for example, CH_4 selectivity, CO conversion, CO_2 capacity and absorption rate, and the stability of the mixed bed during multiple carbonation and decarbonation cycles.

4.2 Results and Discussion

4.2.1 Thermodynamic Equilibrium Calculation of Methanation in the Absence of Carbon Dioxide Sorption

Syngas methanation reactions are limited by thermodynamic equilibrium. The equilibrium gas composition was determined based on a closed isothermal system in which the feed gas components, the composition, and the reaction conditions (temperature, pressure, etc.) are given. In the absence of CO_2 sorption, two closed isothermal systems were studied for the consideration of both dry methanation and wet methanation reactions. One system contains 0.4 mole of H_2, 0.32 mole of CO, 0.03 mole CH_4, and 0.03 mole N_2, and the other system contains 0.34 mole of H_2, 0.28 mole of CO, 0.19 mole CO_2, 0.15 mole of H_2O, 0.023 mole CH_4, and 0.026 mole of N_2. Nitrogen was considered to be inert. Figure 4.2 shows the calculated CO conversion and the selectivity of CO_2 and CH_4 for the two systems. As shown in Figure 4.2(a), the CO conversion shows slight decrease as the temperature increases in the first system. For example, CO conversion decreases from 99.6% to 94.6% when the reaction temperature increases from 300 to 400ºC. Equilibrium selectivity for both CO_2 and CH_4 remains almost constant at 64% and 36% in the temperature range of 300 to 400ºC, respectively. Figure 4.2(b) shows the calculated CO conversion and the equilibrium selectivities of CO_2 and CH_4 when including water in the syngas. The addition of 15 mol% water to syngas caused a slight increase in CO conversion for all temperatures studied.

4.2.2 Sorbent Performance Results

The regeneration and stability of the sorbents were first assessed using TGA by carrying out continuous multiple CO_2 absorption and desorption cycles under dry conditions as reported in Chapter 3. Optimal temperatures were determined by conducting initial trial tests at various temperatures. The temperatures that provided a combination of high capacity and fast absorption-desorption rates were selected. Figure 4.3 shows the performance results for the three sorbents with the mass at the start of cycles set to 100%. Of the three sorbents, Sorbent-3 shows the best stability and highest CO_2 capacity during eight cycles.

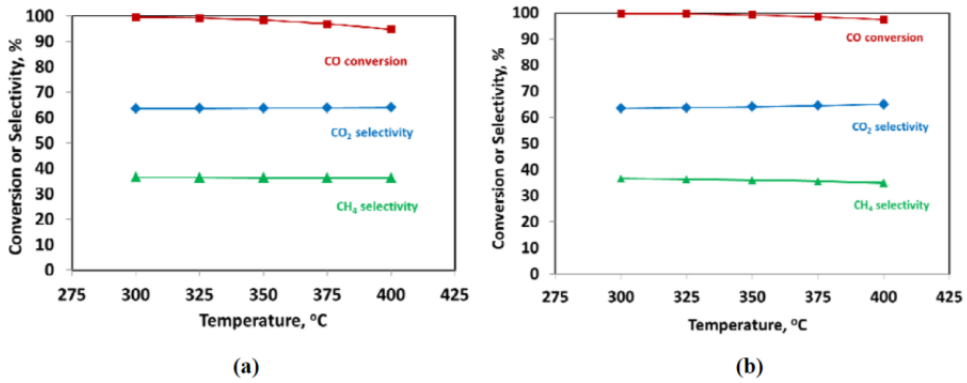

Figure 4.2. Thermodynamic Equilibrium CO Conversion, CO_2 Selectivity, and CH_4 Selectivity in the Temperature Range of 300 to 400ºC at Ambient Pressure. (a) System containing 40% H_2, 32% CO, 22% CO_2, 3% CH_4, and 3% N_2. (b) System containing 34.2% H_2, 28.2% CO, 18.8 CO_2, 15% $_{H2}O$, 2.6% CH_4, and 2.6% N_2.

Table 4.1summarizes the CO_2 sorption capacity (in mmol/g) and measured average sorption rates of the three sorbents. One can see that the first cycle absorption rate is always the highest during eight cycles for all the sorbents. The absorption rate from the second cycle through the eighth cycle varies in a small range. For all the sorbents, the desorption rate seems to be stable during the multiple cycles.

Breakthrough performance of the three sorbents was assessed in a fixed-bed reactor with a gas stream containing 60% CO_2 and 40% N_2. For each sorbent, feed gas space velocity was first varied to obtain the optimal condition for the sorbent breakthrough tests. Figure 4.4(a-c) shows the CO_2 concentration detected in the gas phase as a function of time during the sorption breakthrough tests of the three sorbents.

For Sorbent-3, CO_2 was detected at 54 minutes, and its concentration remained at 19.2% for 150 minutes, followed by a long and slow increase until the sorbent became saturated with CO_2 at about 1,000 minutes. The total carbonation lasted ~950 minutes before reaching the saturation state. Figure 4.4(d) shows the corresponding CO_2 absorption rate (mmol/g/min) and estimated CO_2 sorption capacity for the three sorbents. The CO_2 absorption rate of Sorbent-1 increased rapidly with time and reached a maximum of 0.056 mmol/g/min, and then a gradual decrease occurred over time down to zero at ~400 minutes. The CO_2 sorption capacity was estimated to be ~12.4 mmol/g (or 54.5 wt%). Sorbent-2 and Sorbent-3 show similar absorption rates at the beginning, and their CO_2 sorption rates reached the maximum almost at the same time. However, compared to Sorbent-2, Sorbent-3 has a longer duration of slow absorption at the later stage of CO_2 sorption. The estimated CO_2 sorption capacity for Sorbent-2 and Sorbent-3 is 3.0 mmol/g (in cycle 5) and 9.84 mmol/g (in cycle 3), respectively. For all sorbents, the measured CO_2 capacity from the fixed-bed tests is generally lower than that obtained by TGA, possibly because of the temperature gradient present in the fixed-bed reactor.

(a)

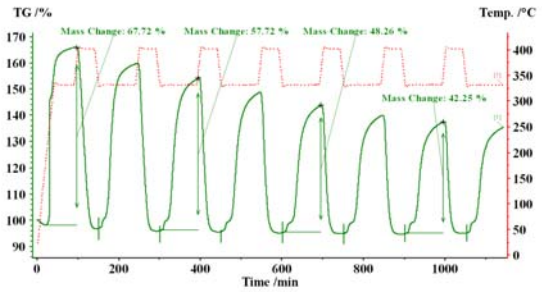

(b)

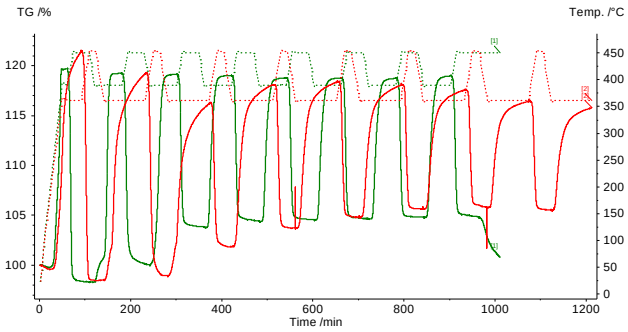

Green: 390C (60 min), 450C (60min)
Red: 360C (90min), 450C

(c)

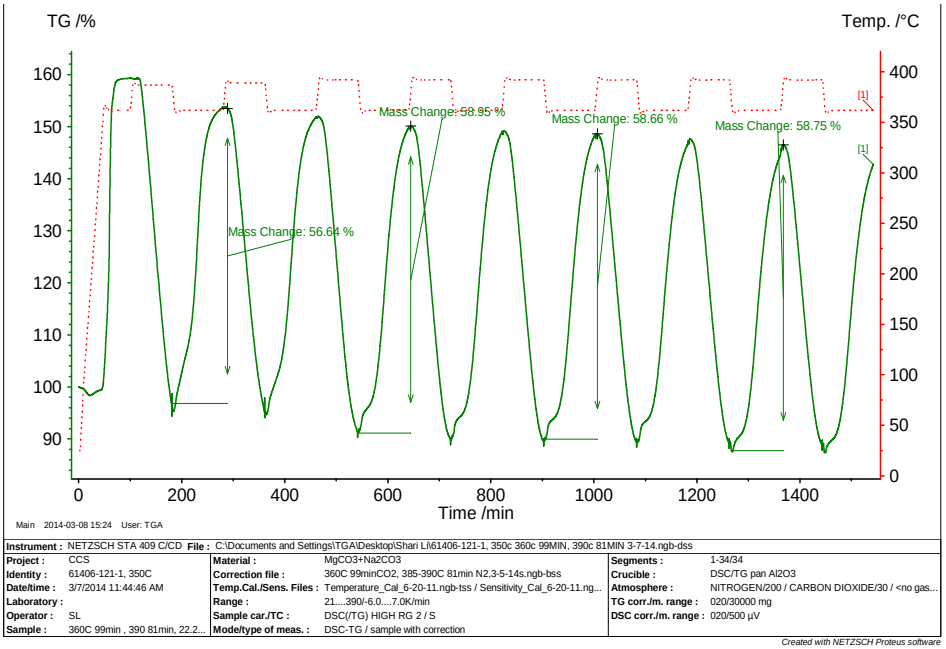

Figure 4.3. Multi-Cycle CO_2 Absorption-Desorption Performance of (a) Sorbent-1, (b) Sorbent-2, and (c) Sorbent-3 by the Combined Temperature/Pressure Swing Operation in a TGA Apparatus. The temperature and feed gas used for the carbonation and decarbonation cycles are between 330°C in CO_2 and 400°C in N_2 for Sorbent-1, between 360°C in CO_2 and 450°C in N_2 for Sorbent-2, and between 360°C in CO_2 and 390°C in N_2 for Sorbent-3.

Table 4.1. Summary of CO_2 Sorption Capacity and Calculated Absorption/Desorption Rates of Three Types of Sorbents using Combined Temperature and Swing Pressure Operation in a TGA Apparatus

Sorbent ID		-1	-2	-2	-3
Type of molten salts		$NaNO_3$	LiNaK-CO_3 eutectic salt	LiNaK-CO_3 eutectic salt	LiNaK-CO_3 eutectic salt
Operation condition	carbonation	330°C in CO_2	390°C in CO_2	360°C in CO_2	360°C in CO_2
	decarbonation	400°C in N_2	450°C in N_2	450°C in N_2	390°C in N_2
Cycles 1–8 capacity, mmol/g		6–14	3.3–4.5	2.4–5	13–15
First cycle CO_2 absorption rate, mmol/g/min		0.23	0.19	0.18	0.9
Cycles 2-8: Average CO_2 absorption rate, mmol/g/min		0.18–0.2	0.12–0.16	0.06–0.14	0.16–0.2
Cycle 3-8: Average CO_2 desorption rate, mmol/g/min		0.3–0.35	0.23	0.23	0.17–0.2

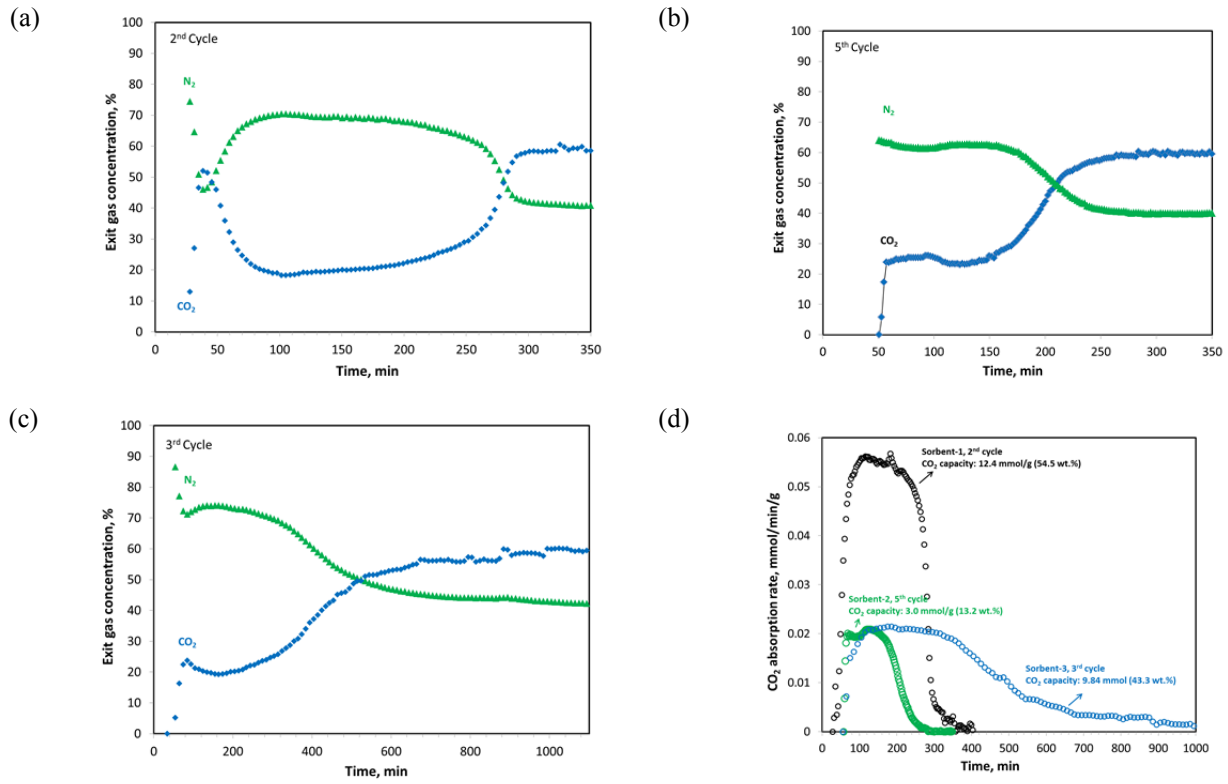

Figure 4.4. Measured Breakthrough Performance for (a) Sorbent-1, (b) Sorbent-2, and (c) Sorbent-3, and the Comparison of Measured Absorption Rate with Time-on-Stream in (d). All tests were operated in a fixed-bed reactor using the feed gas 60% CO_2/40% N_2. Testing conditions: (a) carbonation at 328°C, regeneration at 400°C in N_2 for 1 hour, gas hourly space velocity (GHSV) = 103 hour^{-1}; (b) carbonation at 390°C, regeneration at 450°C in N_2 for 1 hour, GHSV = 41 hour^{-1}; and (c) carbonation at 328°C, regeneration at 390°C in N_2 for 1.2 hours, GHSV = 41 hour^{-1}.

4.2.3 Integrated Syngas Methanation and Carbon Dioxide Capture

4.2.3.1 Sequential Bed Integration Performance Results and Characterization

Sorbent-1 was first selected for the integrated test in the sequential bed. Before the integrated test, the reactivity and stability of methanation catalyst were evaluated as a baseline at 330°C without sorbent. Figure 4.5(a) shows the measured CO conversion and the selectivities of CH_4 and CO_2 as a function of time during the methanation. We found that complete conversion of CO was achieved at 330°C over the 20% $Ni/MgAl_2O_4$ catalyst. In addition, the methanation reaction could reach stability in less than 20 minutes during which the measured selectivities of CO_2 and CH_4 reached their respective thermodynamic equilibrium values. A separate 50-hour stability test shows that the catalyst was stable for the methanation process. Integrated tests in the sequential bed were performed with a dry syngas stream containing 37% H_2, 30% CO, 2.7% CH_4, 21.5% CO_2, and 8.8% N_2 at 330°C and 1 bar, and the results are shown as a function of time in Figure 4.5(b). Complete CO conversion and gas phase selectivity to CH_4 of >80% was achieved and maintained for ~100 minutes. For the integrated test, CO_2 was detected in the exit gas during carbonation, suggesting that CO_2 cannot be completely absorbed before leaving the reactor, possibly because of the restriction of the equilibrium CO_2 partial pressure of reaction 4.3. After ~120 minutes time-on-stream, the sorbent became saturated with CO_2. The CO_2 sorption capacity of the sorbent was estimated to be ~8 mmol/g (~44.8 wt%). Upon reaching CO_2 sorption capacity, the gas phase CH_4 selectivity dropped to 34%, while the gas phase CO_2 selectivity increased to 66%, with both approaching the equilibrium values. The integrated test in the sequential bed thus demonstrated that the CH_4 yield could be increased from its equilibrium value of 34% up to >80% because of the enhancement of CO_2 sorption.

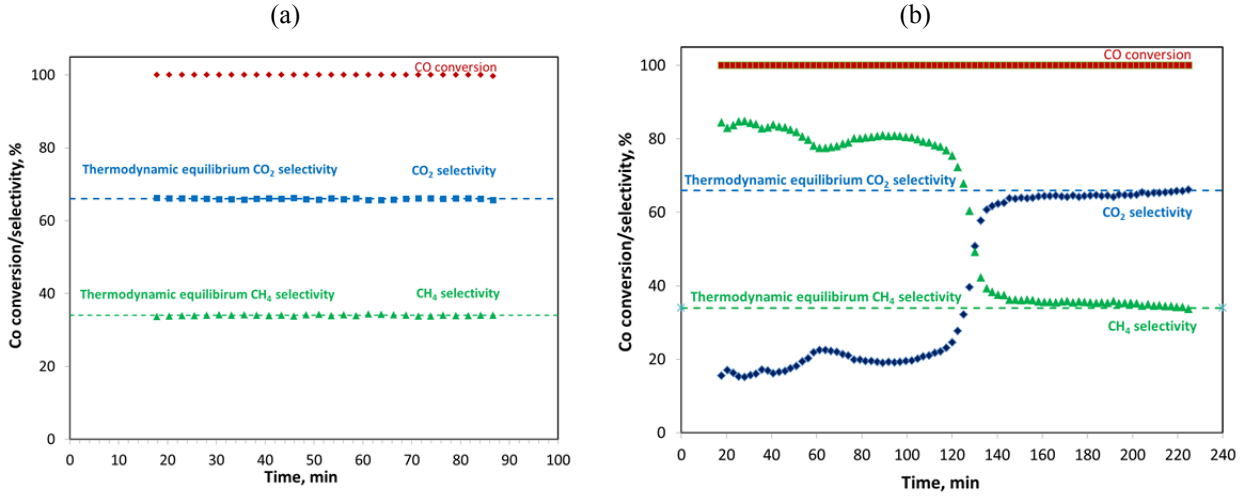

Figure 4.5. Variation of CO Conversion and Gas Phase Selectivity to CO_2 and CH_4 as a Function of Time-on-Stream for (a) the Methanation Reaction Only, (b) the Fifth Cycle Of The Integrated Methanation Reaction with CO_2 Capture (Sorbent-1) in a Sequential Bed. Testing conditions: catalyst = 20wt% $Ni/MgAl_2O_4$; feed gas =37% H_2, 30% CO, 2.7% CH_4, 21.5% CO_2, and 8.8% N_2; pressure = 1 bar; temperature = 330°C; GHSV_methanation = 12,000 $hour^{-1}$; and GHSV_sorption = 260 $hour^{-1}$.

Figure 4.6 shows the representative SEM images of the three samples.

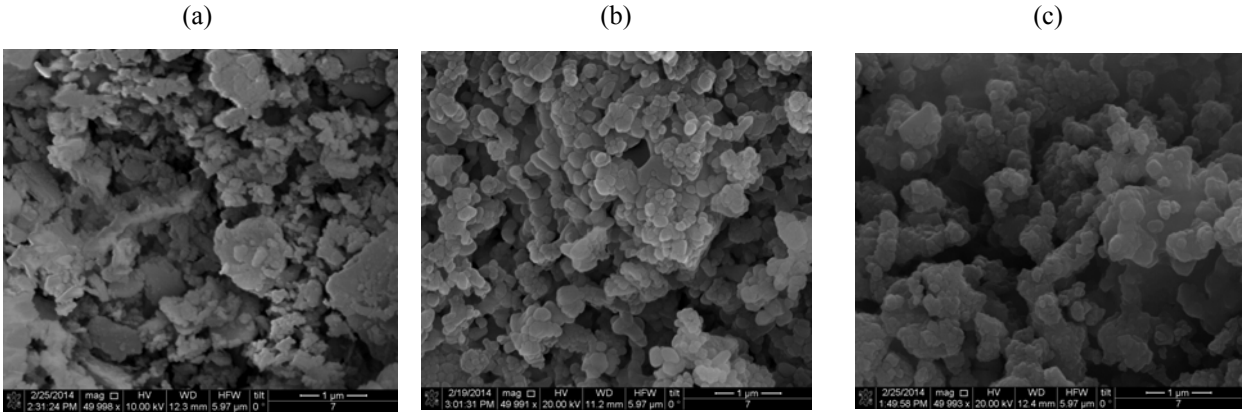

Figure 4.6. Comparison of SEM Morphologies of Sorbent. (a) Fresh sorbent-1, (b) after first cycle of carbonation, and (c) after eighteenth decarbonation cycle.

4.2.3.2 Mixed-Bed Integration Performance Results and Characterization

Mixed-Bed Integrated Test at Ambient Pressure

Proof-of-concept studies of integrating syngas methanation reaction with in situ CO_2 capture were first carried out at ambient pressure in a mixed-bed that consisted of a mixture of 20 wt% $Ni/MgAl_2O_4$ and Sorbent-2. To understand the role of water on integration performance, two scenarios—including feed with and without water—were considered in this work.

When water was not included in the feed, the syngas feed was composed of 40% H_2, 32% CO, 22% CO_2, 3% CH_4, and 3% N_2. Before the integrated tests, the methanation reaction without CO_2 capture was performed at 360°C, and the results as a function of time-on-stream are given in Figure 4.7(a). Similar to the syngas methanation reaction without sorbent at 330°C, a complete CO conversion was achieved at 360°C, and the selectivities to CH_4 and CO_2 reached their equilibrium values of 36% and 64%, respectively, in less than 50 minutes. The catalyst shows fairly stable performance during the 12-hour test. The integrated tests were performed at the same temperature and the same space velocity as those for the methanation reaction without sorbent, and the results are given in Figure 4.7(b). It is seen that a complete CO conversion and selectivity to CH_4 of up to 77.2% were achieved. The maximum level of CH_4 selectivity maintained about 50 minutes, followed by a gradual decrease with time possibly because of the slowdown of the absorption rate. After about 460 minutes of carbonation, the sorbent became saturated with CO_2, and it was calculated that the sorbent reached a capacity of 2.7 mmol/g (~11.7 wt%).

When water was included in the syngas, the feed was composed of 34% H_2, 27.2% CO, 18.7% CO_2, 2.55% CH_4, 2.55% N_2, and 15% H_2O. A 40-hour reactivity and stability test of the syngas methanation reaction without sorbent was performed first over the 20 wt% $Ni/MgAl_2O_4$ catalyst at 360°C, and the results are given in Figure 4.8(a). The CO conversion was 98% at the beginning and remained at that level for ~8 hours, followed by a drop to 93.4% at 13 hours. After that, the CO conversion recovered to

96.4% at 28 hours and remained at that level until the completion of the test. The selectivities of CO_2 and CH_4 reached their equilibrium values in less than 2 hours and remained almost constant during the entire experiment. The integrated testing results are shown as a function of time in Figure 4.8(b).

(a) (b)

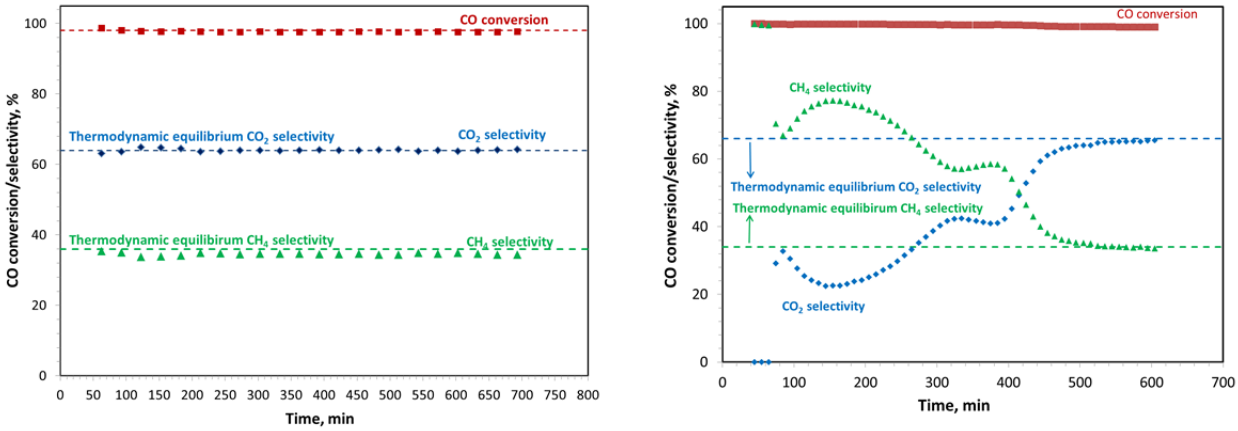

Figure 4.7. Variation of CO Conversion and Gas Phase Selectivity to CO_2 and CH_4 as a Function of Time-on-Stream for (a) the Dry Methanation Reaction Only, (b) the Second Cycle of the Integrated Methanation Reaction with CO_2 Capture (Sorbent-2) in a Mixed-Bed Reactor. Testing conditions: feed gas = 40% H_2, 32% CO, 3.0% CH_4, 22% CO_2, and 3.0% N_2; pressure = 1 bar; temperature = 360°C; GHSV_methanation = 1800 $hour^{-1}$; GHSV_sorption = 45 $hour^{-1}$.

(a) (b)

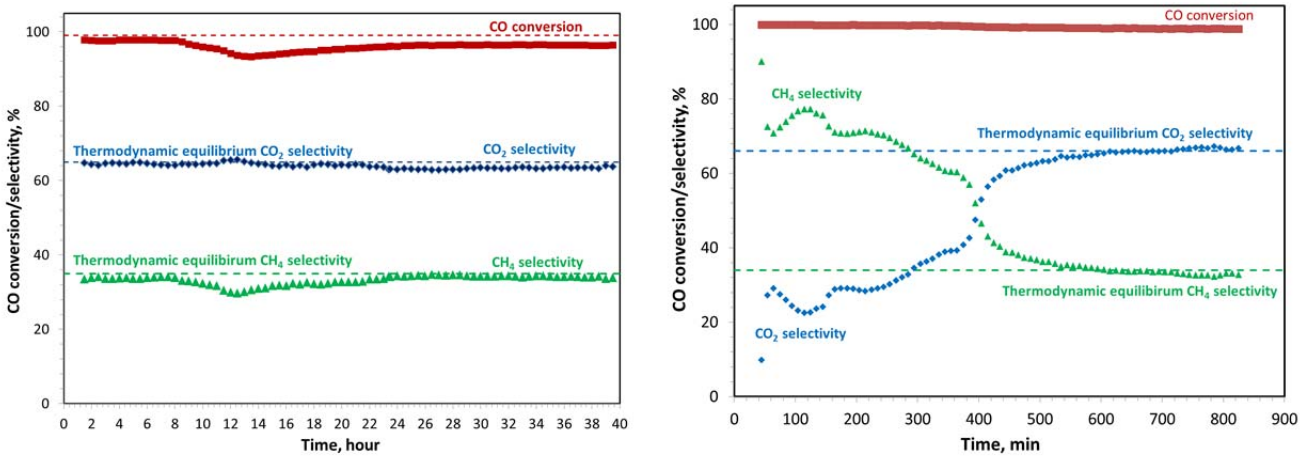

Figure 4.8. (a) Variation of CO Conversion and Gas Phase Selectivity to CO_2 and CH_4 as a Function of Time-on-Stream for (a) the wet Methanation Reaction Only and (b) the Second Cycle Integrated Methanation Reaction with CO_2 Capture in a Mixed-Bed Reactor. Testing conditions: wet feed gas = 15% H_2O, 40% H_2, 32% CO, 3.0% CH_4, 22% CO_2, and 3.0% N_2; pressure = 1 bar; temperature = 360°C; GHSV_methanation = 1800 $hour^{-1}$; and GHSV_sorption = 46 $hour^{-1}$.

The gas phase CH_4 selectivity was at its maximum level of 77.3% for about 40 minutes, after which it gradually decreased possibly because of the decreasing absorption rate of the sorbent. After ~600 minutes, the sorbent became saturated with CO_2, and we calculated that the sorbent had reached a CO_2 capacity of ~5.3 mmol/g (~23.5 wt%), which is almost twice that obtained when water was not included in the feed. In this integrated test, CO_2 was detected in the exit gas during carbonation. Thus, the mixed-bed integrated test successfully demonstrated that the gas phase CH_4 yield could be enhanced from its equilibrium value of ~34% to ~80% under sorption-enhanced conditions in the presence or absence of water in the feed syngas.

Figure 4.9(a) illustrates the effect of the operating temperature and water addition to the feed gas on the gas phase CH_4 selectivity and CO_2 sorption capacity during the integrated tests. In the case where no water was in the feed, the CO_2 sorption capacity increased from 1.6 mmol/g to 3.2 mmol/g as the temperature increased from 335 to 390ºC, while the CH_4 gas phase selectivity dropped from 79.4% to 49%. In the case in which 15 mol% water was present in the syngas, the CO_2 sorption capacity was significantly enhanced (2.6 mmol/g vs. 5.3 mmol/g in cycle 2) at 360°C. At a lower temperature of 335°C, the CO_2 sorption capacity increased from 1.6 to 2.3 mmol/g. In addition, we found that the presence of water in the syngas helped to increase the CH_4 gas phase selectivity from 79.4 to 85.6% at 335°C. For all runs listed in Figure 4.9, CO_2 was detected in the exit gas, and its concentration was found to be strongly dependent on the operating temperature. The higher the operating temperature, the higher the CO_2 concentration detected by Micro-GC in the exit gas. Figure 4.9(b) shows the measured minimum CO_2 partial pressure during carbonation as a function of operating temperature in the presence or absence of water in the feed. The minimum CO_2 partial pressure was determined based on the operation pressure (i.e., 1 bar) and the minimum CO_2 concentration obtained during carbonation. As can be seen, the operation temperature has a significant effect on the measured minimum CO_2 partial pressure. The increase in equilibrium CO_2 partial pressure with temperature can be explained based on reaction 4.5, which is exothermic, thus the increase of temperature would cause the equilibrium to shift to the left side favoring reaction 4.6. Therefore, the increase of operation temperature caused the increase of CO_2 partial pressure in the effluent gas, thus causing the gas phase CH_4 selectivity to decrease. In this case, the reaction thermodynamics can be considered as the main factor controlling the gas phase CH_4 selectivity.

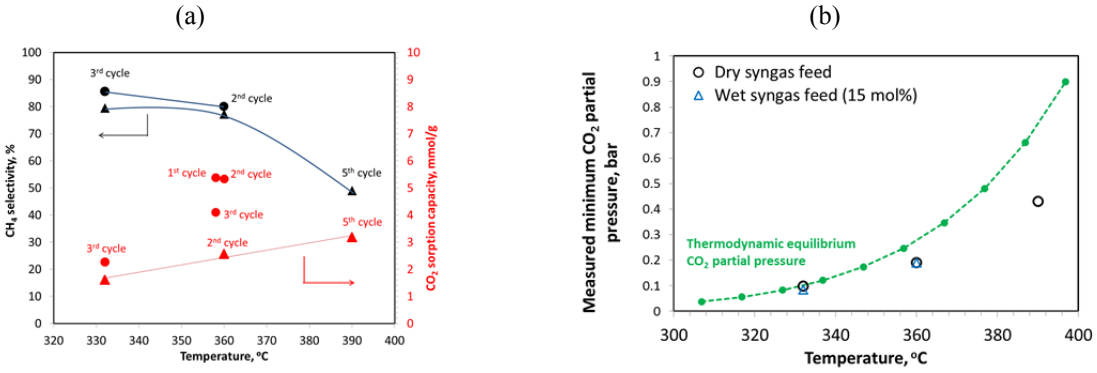

Figure 4.9. (a) Summary of Measured Gas Phase CH_4 Selectivity and CO_2 Sorption Capacity as a Function of the Operation Temperature during Integrated Tests with water in the Syngas Feed (circles) and without Water in the Syngas Feed (triangles); (b) Change of Measured Minimum CO_2 Partial Pressure as a Function of the Operation Temperature. Testing conditions: wet syngas feed = 34% H_2; 27.2% CO, 18.7% CO_2, 2.55% CH_4, 2.55% N_2, and 15% H_2O; pressure = 1 bar; GHSV_methanation = 1800 $hour^{-1}$; GHSV_sorption = 46 $hour^{-1}$; regeneration at 450°C in N_2.

Mixed-Bed Integration Test at an Elevated Pressure

The methanation process commonly operates at elevated pressures to maximize reaction performance. Therefore, the integrated tests were performed at 10 bar using a stainless-steel, fixed-bed reactor containing a mixture of Sorbent-2 and the 20 wt% $Ni/MgAl_2O_4$ catalyst. Carbonation was conducted at 330ºC, both with and without water in the feed. Decarbonation was conducted at 450ºC by flowing 200 sccm N_2 through the reactor for 1 hour. Figure 4.10(a) shows the measured CO conversion, and the gas phase CH_4 and CO_2 selectivity as a function of time when water was not included in the feed syngas. As seen in the figure, complete CO conversion was achieved throughout the entire experiment. The ~99% selectivity to CH_4 (gas phase selectivity) was achieved and maintained for at least 130 minutes. After ~500 minutes of carbonation, the sorbent became saturated with CO_2, and we calculated that the sorbent reached a CO_2 capacity of 16.9 wt%, which is approximately twice the capacity obtained when the process is operated at 1 bar. Upon reaching the CO_2 sorption capacity, the CH_4 gas phase selectivity dropped to 41%, which approaches the equilibrium value. When water was included in the syngas feed, similar integration performance was achieved as shown in Figure 4.10(b). Complete CO conversion was achieved at 330°C throughout the entire experiment. A high gas phase CH_4 selectivity of ~99% was achieved and maintained for ~130 minutes, after which a gradual decrease in selectivity occurred. Carbonation lasted ~567 minutes before the sorbent became saturated with CO_2, and the calculated CO_2 capacity was ~18.3 wt%. After the sorbent reached its capacity, gas phase CH_4 selectivity decreased to 37.8%, which approaches its equilibrium value. Thus, the CO_2 formed was efficiently absorbed by MgO and Na_2CO_3 in accordance with reaction 4.5, and the mixed-bed system was efficient under the operating conditions to convert the syngas feed to CH_4 at a yield of ~99%.

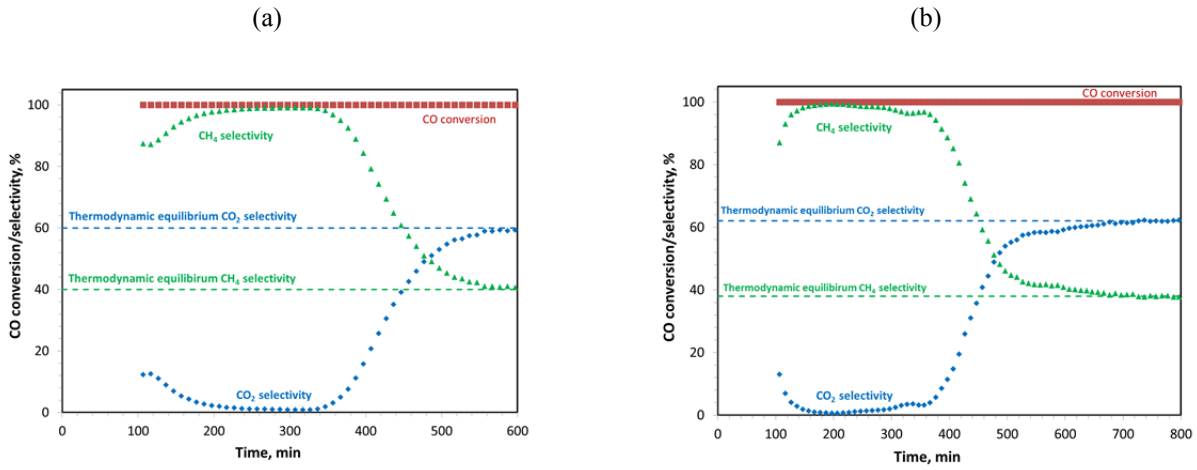

Figure 4.10. Variation of CO Conversion and Gas Phase Selectivity to CO_2 and CH_4 as a Function of Time for (a) the First Cycle of the Integrated Methanation Reaction with CO_2 Capture in a Mixed-Bed Reactor, (b) the Third Cycle of the Integrated Wet Methanation Reaction with CO_2 Capture in a Mixed-Bed Reactor. Testing conditions: wet gas feed wet gas = 15% H_2O, 40% H_2, 32% CO, 3.0% CH_4, 22% CO_2, and 3.0% N_2; pressure = 10 bar, temperature = 332°C, GHSV_methanation = 1800 $hour^{-1}$, GHSV_sorption = 46 $hour^{-1}$.

Figure 4.11 compares the CO_2 absorption rates as a function of time for the first three cycles of one integrated test at 10 bar and the third cycle of one integrated test at 1 bar. All integrated tests shown in the figure were conducted at 330ºC. As can be seen, all plots show similar behavior with time: the CO_2 absorption rate increases quickly with time reaches a plateau for a period of a few hundred minutes, and then decreases until CO_2 sorption stops. For the three cycles tested at 10 bar, the CO_2 sorption rates were approximately twice the rates from tests at 1 bar (~ 0.012 mmol/g/min vs. 0.0063 mmol/g/min for the third cycle without water in the feed). This shows that the CO_2 sorption rate can be enhanced at higher operating pressures, likely because of the increased driving force for CO_2 sorption onto sorbent surfaces. The inset figure illustrates the estimated CO_2 sorption capacity for the four tests. As shown in the figure, the CO_2 sorption capacity of the sorbent improved significantly when the integrated test was conducted at 10 bar relative to 1 bar because of the increased CO_2 sorption rate at higher pressures. In addition, the results reconfirms that the presence of water in the syngas feed helps to increase the CO_2 capacity.

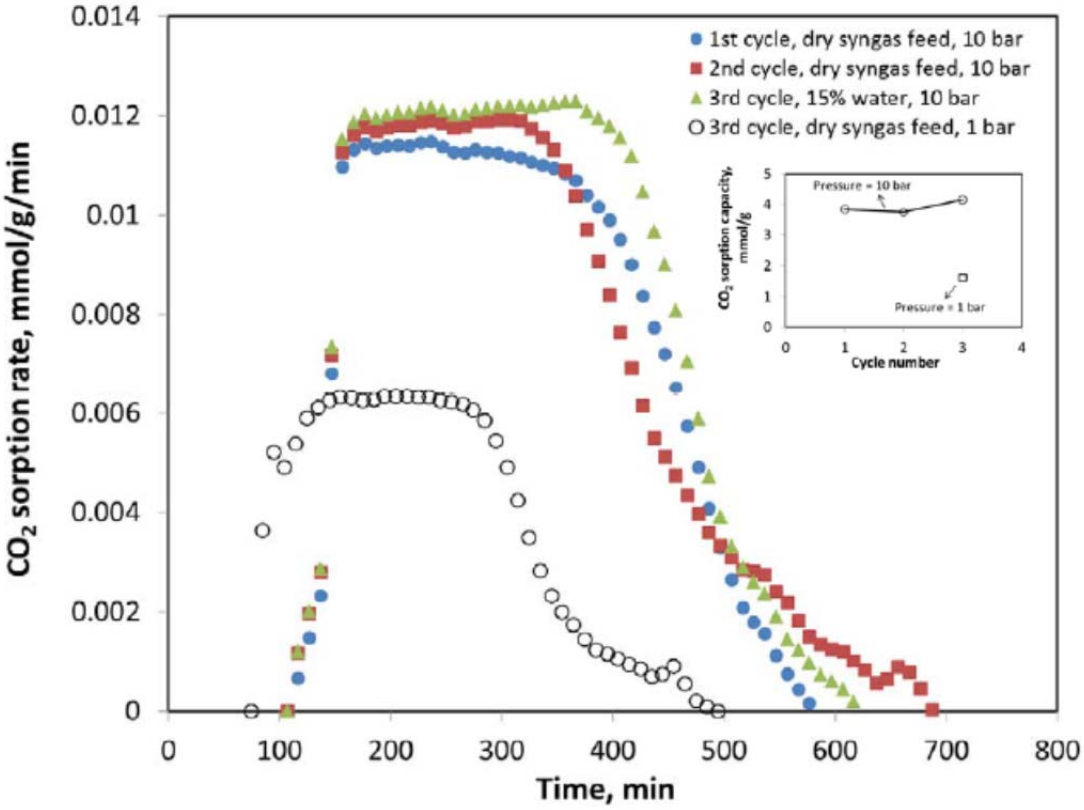

Figure 4.11. Comparison of CO_2 Absorption Rate as a Function of Time during the Mixed-Bed Test of Sorbent-2 at 10 bar (solid circles) and at Ambient Pressure (open circles). Testing conditions: wet syngas feed = 34% H_2, 27.2% CO, 18.7% CO_2, 2.55% CH_4, 2.55% N_2, and 15% H_2O; temperature = 332ºC; GHSV_methanation = 1800 $hour^{-1}$; GHSV_sorption = 46 $hour^{-1}$; and regeneration at 450°C in N_2 for 1 hour.

4.3 Conclusions

In this work, we investigated an integrated process for producing CH_4-rich gases. The integrated process combined a syngas methanation catalyst of 20 wt% $Ni/MgAl_2O_4$ with a molten-phase promoted MgO-based sorbent. We demonstrated that a significant increase of CH_4 yield was achieved by combining syngas methanation, WGS, and CO_2 capture in a single reactor. Through integration, the CH_4 yield can be increased from 32 to 86% when tested at 1 bar and 335°C and from 40 to >99% when tested at 10 bar and 332ºC. In addition, the CO_2 capacity of the sorbent increased when 15 mol% of water was present in the syngas feed; this improvement in capacity was the result of enhanced CO_2 sorption rates. The stability of catalyst and Sorbent-2 when combined in a mixed-bed was studied over multiple carbonation and decarbonation cycles. We found that both the sorbent and the catalyst show favorable stability after multiple test cycles.

5.0 Warm Inorganic Contaminant Cleanup

5.1 Introduction

Gasifier-derived syngas must be treated to remove a number of impurities that would otherwise poison the synthesis catalysts(s). Inorganic impurities include alkali salts, chloride, sulfur compounds, heavy metals, ammonia, and various phosphorus-, arsenic-, antimony-, and sulfur-containing compounds (Torres et al. 2007). Many of these must be removed to part per billion levels because of their strong, detrimental interaction with downstream WGS and synthesis catalysts. In this section, we describe the sorbents necessary for the removal of hydrogen chloride (HCl) and sulfur, and a multi-functional sorbent useful for the removal of a variety of contaminants.

5.2 Hydrogen Chloride Cleanup

The sorption capacities of HCl were investigated previously as a function of temperature using Na_2CO_3 sorbent and simulated syngas (containing 100 ppm HCl). As reported in our earlier publication for biomass application and as depicted in Figure 5.1, an optimal sorbent capacity was found when operating at 450ºC and 500ºC (Howard et al. 2013). Thus, for the cleanup of HCl, a Na_2CO_3 bed was used and operated at 450ºC.

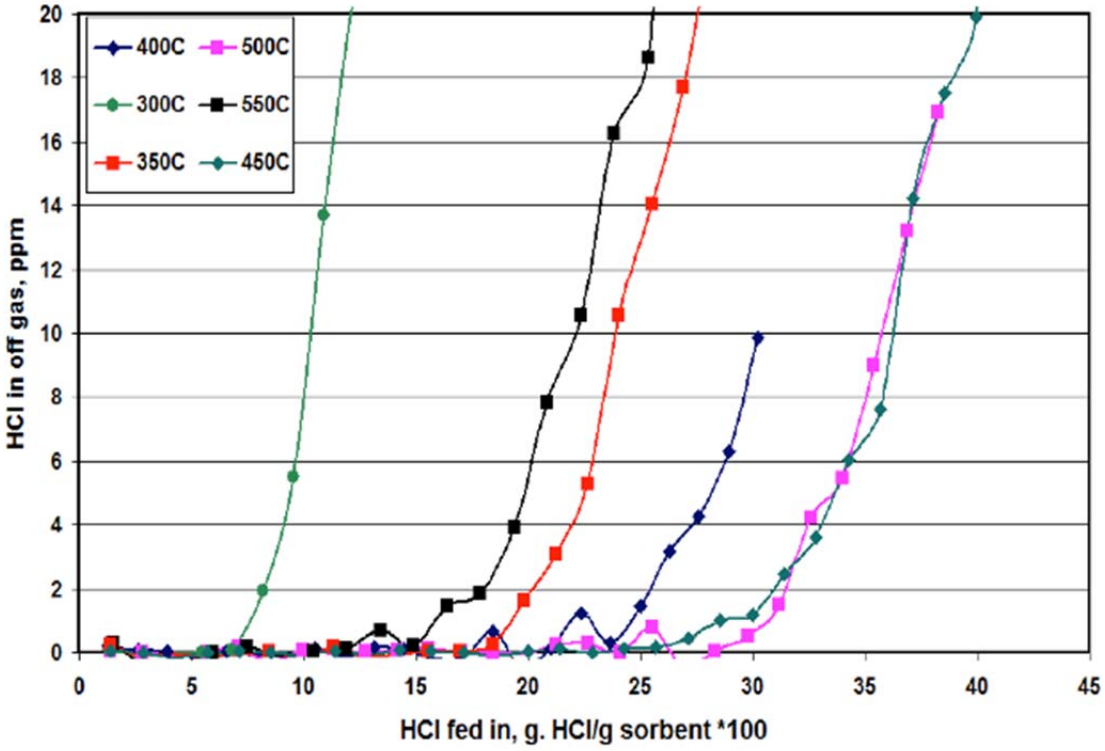

Figure 5.1. HCl Sorption Capacities as a Function of Temperature using a Simulated Syngas and Na_2CO_3 Operating under the Following Conditions: 50% H_2O, 13% CO, 10% CO_2, 20% H_2, 7% CH_4, 100 ppm HCl 80,000 hr^{-1}, 1 atm. Reprinted with Permission from Howard et al. 2013.

5.3 Sulfur Cleanup

Zinc oxide can react with both H_2S and COS exothermally to produce zinc sulfide (ZnS) (see reactions 5.1 and 5.2) (Xiao et al. 2012).

$$ZnO + H_2S = ZnS + H_2O \quad (5.1)$$

$$ZnO + COS = ZnS + CO2 \quad (5.2)$$

As shown in Figure 5.1, concentrations of total sulfur species less than 100 ppbv can be achieved under thermodynamic equilibrium in real syngas operating conditions. Sasaoka and co-workers experimentally found that increasing the amount of H_2O had a larger negative impact on the adsorption of H_2S on ZnO then CO_2 even with the formation of COS (Sasaoka et al. 1994, 1996; Sasaoka 1995). They also found that a system with only COS and ZnO will produce CO_2, ZnS, and some elemental sulfur (Sasaoka 1995). While there is evidence of COS adsorption, results from experiments conducted at 150ºC and 200ºC revealed no COS adsorption, indicating that there is a substantial activation energy for COS hydrolysis (Li and King 2006). A thermodynamic equilibrium model based on H_2S and COS in syngas with ZnO is provided in Table 5.1.

Table 5.1. Thermodynamic Equilibrium Model of H_2S and COS

		Temperature,					
		300ºC	350ºC	400ºC	450ºC	500ºC	550ºC
H_2	%	50.03	48.07	45.96	43.91	41.92	40.08
CO_2	%	35.20	33.24	31.12	29.07	27.10	25.26
CO	%	10.64	12.58	14.74	16.79	18.71	20.55
H_2O	%	4.13	6.11	8.19	10.24	12.27	14.11
H_2S	ppbv	1.71	8.99	35.62	113.61	304.70	716.77
COS	ppbv	0.03	0.18	0.76	2.64	7.75	19.73

Regeneration of ZnO can be represented by reaction 5.3. However, there are three concerns with ZnO regeneration: 1) formation of zinc sulfate ($ZnSO_4$), 2) formation of zinc metal, and 3) changes in the atomic structure. Under regeneration conditions, undesired $ZnSO_4$ can be formed by reactions 5.4 and 5.5 (Xiao et al. 2012). Formation of $ZnSO_4$ is undesirable because it is highly stable and will not easily reconvert to ZnO. Experimental work exploring ZnO regeneration has found that temperatures of 650ºC and O_2 concentrations around 2% help to minimize the formation of sulfate (Xiao et al. 2012). In addition, the combination of other oxides with the ZnO particularly titanium oxide have been observed to help decrease the formation of $ZnSO_4$ (Elseviers and Verelst 1999).

$$ZnS + 1.5O_2 = ZnO + SO_2 \quad (5.3)$$

$$ZnO + SO_2 + 0.5O_2 = ZnSO_4 \quad (5.4)$$

$$ZnS + 2O_2 = ZnSO_4 \quad (5.5)$$

Another concern for the ZnO lifetime is the formation of zinc metal by the reduction of ZnO under the reducing conditions of the syngas. Experiments have shown zinc reduction is significant at temperatures above 650ºC (Elseviers and Verelst 1999), Lew et al. 1992). Fortunately, the presence of other metal oxides that are used to decrease sulfate formation also helps stabilize the material against reduction (Elseviers and Verelst 1999).

While the surface area of the ZnO is not thought to be the controlling factor in adsorption of sulfur, regeneration can lead to changes in the internal structure of the sorbent surface area, which may reduce the effectiveness of the absorbent by reducing transport rates (Zhao et al. 2007, Efthimiadis and Sotirchos 1993, Davidson et al. 1989). When the ZnS is formed, its crystal structure becomes warped because of the significantly larger size of the sulfur atom relative to the oxygen (O_2) atom (Winter 2012). Repeated desulfurization experiments with varying particle sizes of sorbent found a similar initial capacity but a significant decrease in capacity when larger particles were used (Efthimiadis and Sotirchos 1993). Davidson et al. (1989) observed that particle size had a larger impact on kinetics than temperature because of the diffusion of sulfur through the ZnS "shell" (Davidson and Sohail 1995).

While ZnO-based sorbents have significant promise, the material has been described to be less effective in removing COS (Sasaoka et al. 1996). The presence of COS is common in syngas because it is in thermodynamic equilibrium with other gas species (see reactions 5.6 and 5.7). Experiments have shown that COS reacting directly with ZnO (see reaction 5.2) is highly unfavorable, so only through conversion to H_2S can the sulfur be adsorbed (Graedel et al. 1981, Rhodes et al. 2000).

$$CO + H_2S = COS + H_2 \qquad K_{eq} = 8.5 \times 10^{-2} \tag{5.6}$$

$$CO_2 + H_2S = COS + H_2O \qquad K_{eq} = 2.1 \times 10^{-3} \tag{5.7}$$

Under typical warm gas cleanup conditions (450ºC), the equilibrium of reactions 5.6 and 5.7 are on the H_2S side. The hydrolysis of COS, which is the reverse of reaction 5.7, is the most likely pathway for COS conversion. Studies have shown that secondary metal oxides including aluminum oxide (Al_2O_3), ZrO_2, and titanium oxide as well as ZnS can catalyze the COS hydrolysis reaction (Sasaoka et al. 1996). Because the sulfur in COS is can be adsorbed directly or through an intermediate as H_2S, the overall sulfur slip is controlled both by the thermodynamics of reactions 5.1, 5.2, 5.6, and 5.7, but also sufficient kinetics and transport exist to push the system toward thermodynamic equilibrium. Because the structure of the adsorbent is expected to change after regeneration, understanding the impact of those changes on the kinetics and transport is a key factor to understanding the effectiveness of ZnO-based desulfurization sorbents.

Because the overall goal of our desulfurization work is economical, effective removal of sulfur from syngas generated from coal gasification, we studied commercially available ZnO sorbents. The two sorbents used in this study were G-72D (Actisorb 2) and G-72E (Actisorb 3) available from Clariant. Both sorbents contain 90 ±3% ZnO along with a proprietary mixture of metal oxides. Generally, it is known that these additional oxides are a combination of Al_2O_3, ZrO_2, and titanium oxide that are different for the two sorbents. By using a highly accurate SCD attached to a GC instrument, we were able to determine sulfur elution from the bed to levels <50 ppbv and also its molecular source. Our goal was to determine whether, and under what conditions, a commercially available ZnO sorbent is capable of removing sulfur gases to <100 ppbv.

Experiments with warm gas cleanup for IGCC applications indicate that while ZnO sorbents are highly effective at removing sulfur at 450ºC, they cannot completely capture everything (i.e., a small amount of sulfur remains) (Yiao et al. 2012). However, our experiments indicate that fresh ZnO operating at lower temperature is highly effective in reducing ZnO levels to below the detection limit of our system (Howard et al. 2013). In this report, we describe studies undertaken to clarify the performance of ZnO, especially fresh ZnO, in removing sulfur gases from wet syngas streams. We have especially been concerned with the behavior of COS in this system, and if it is a limiting factor in overall sulfur gas removal performance.

For the application of ZnO sorbents for desulfurization, we believed there were three areas that needed further study: 1) the temperature impact of H_2S adsorption, 2) the impact of COS, and 3) the impact of regeneration on sulfur adsorption.

5.3.1 Temperature Effects of Hydrogen Sulfide Adsorption

As predicted by thermodynamics, the temperature of adsorption had a significant impact on the adsorption capacity of the G-72D ZnO (see Figure 5.2). While this was not unexpected for the temperatures of 300ºC and 450ºC, because of the temperature dependency of sulfur diffusion inside ZnO, the decrease in capacity at 550ºC was unexpected. This decrease in capacity may be related to surface loss from sintering of the ZnO at a higher temperature, however, because surface adsorption of H_2S on ZnO is not the rate limiting step (Howard et al. 2013), the external surface area of the sorbent is not expected to contribute significantly to the overall capacity. Other metal oxides present in the sorbent may have a negative impact on the H_2S capacity at higher temperatures (Elseviers and Verelst 1999).

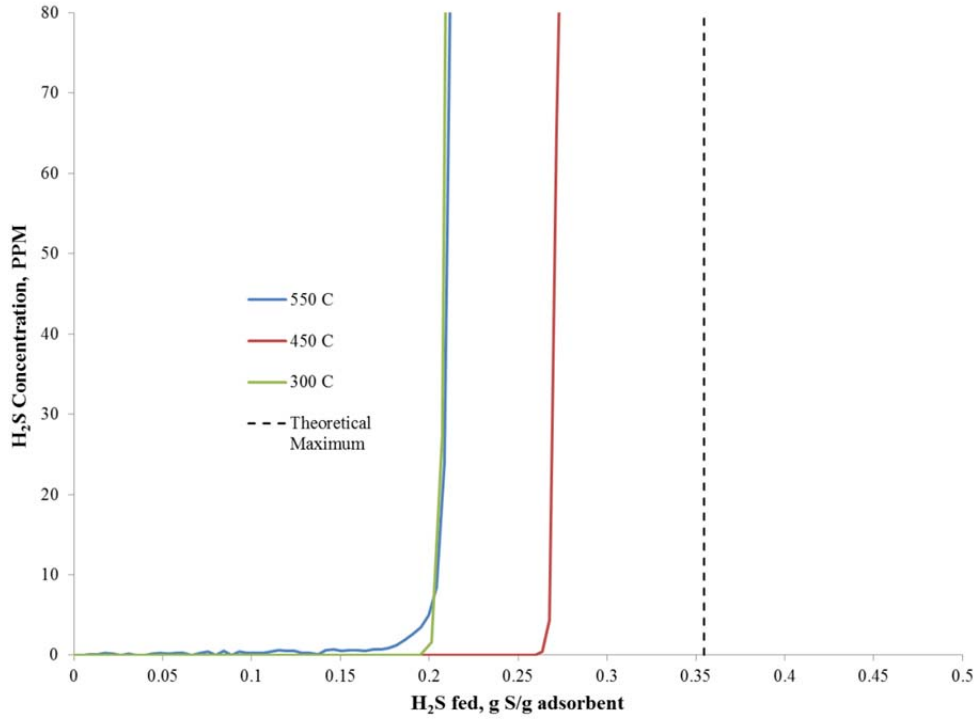

Figure 5.2. Temperature Impact of H_2S Adsorption. H_2S feed concentration = 3,000 ppm, sorbent G-72D, carrier gas: 38.4% CO, 38.4% H_2, 3.2% N_2, 20% H_2O, 450ºC, 12,000 hour^{-1} GHSV.

The equilibrium concentration of H_2S slipping through the reactor as a function of temperature (Figure 5.2) is at, or lower than, thermodynamics would predict. The equilibrium concentration of H_2S at 300ºC and 450ºC were below detection limit (i.e., <50 ppb H_2S). At 550ºC, the experimental equilibrium concentration was just less than 1 ppmv H_2S. Calculations based on thermodynamic principles for H_2S adsorption with syngas and 20% water predict 1.71 ppbv, 113.6 ppbv, and 716.8 ppbv for 300, 450, and 550ºC, respectively. These low concentrations are similar to those observed by other researchers (Gupta et al. 2001, Tamhankar et al. 1986, Lew et al. 1989). The conclusion from this study is that the maximum capacity for sulfur for this sorbent is at or around 450ºC.

5.3.2 Carbonyl Sulfide Adsorption

Carbonyl sulfide, which can be in syngas because of a reaction between H_2S and CO (see reaction 5.6), is hypothesized to be a problem for desulfurization using ZnO because COS will not readily react with ZnO to form ZnS (Sasaoka et al. 1996). Research reported in the literature suggests that COS can be removed by adding water to the feed gas to hydrolyze the COS to H_2S, which can be more easily reacted with ZnO. Our experiments with COS absorption support the conclusion that water assists in COS removal via hydrolysis (see Figure 5.3). At 450ºC, the test with wet COS and wet COS with H_2S behave almost identically indicating the hydrolysis reaction has no impact on the capacity or equilibrium concentration of gas phase sulfur species.

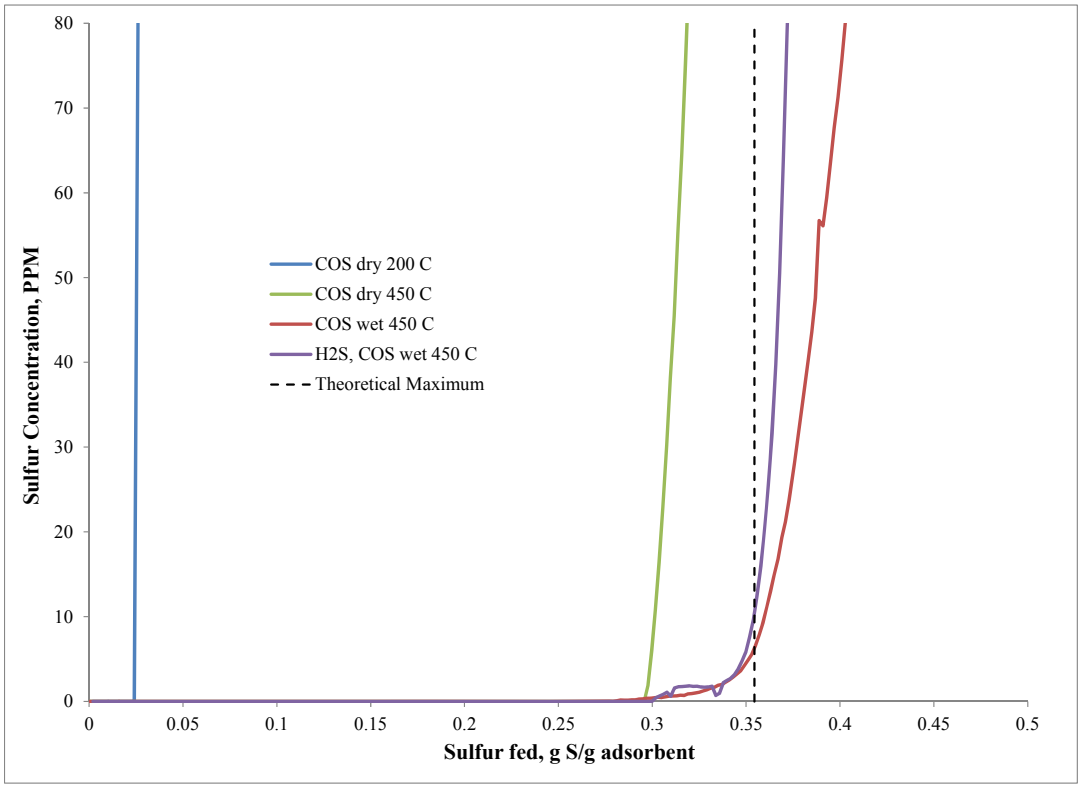

Figure 5.3. Temperature and Water Impact of Carbonyl Sulfide Adsorption. Sulfur feed concentration 1,000 ppm, N_2 carrier gas, sorbent G-72E, 20% H_2O, 450ºC and 200ºC, 12,000 $hour^{-1}$ GHSV

Under dry conditions, there was approximately a 15% decrease in adsorption capacity at 450°C. The presence of any adsorption capacity is an unexpected result because of the absence of water in the system to cause hydrolysis. However, water is a product of the reaction of H_2S with ZnO (reaction 5.1); therefore, small quantities of water in the system that are not consumed may be responsible for COS hydrolysis. In addition, there may be a second route for the adsorption of COS on ZnO that has high activation energy and is only viable at 450ºC. The low-temperature result has been seen before in published literature that reports COS to be mostly unreactive in dry environments and difficult to remove (Graedel et al. 1981, Rhodes et al. 2000, Meng et al. 2009).

5.3.3 Zinc Oxide Regeneration Impacts on Adsorption

The economics of desulfurization require that the oxide used to remove sulfur from syngas must be regenerable. The impact on the adsorption capacity and equilibrium gas phase sulfur concentration has not been well studied. For the experiments performed here, the ZnO sorbent was regenerated at 650ºC with a gas mixture of 5% O_2 and 95% N_2 for 8 hours. The capacity of the sorbent decreased by about 25% over the course of the first two adsorption experiments before settling on a steady state adsorption capacity (see Figure 5.4).

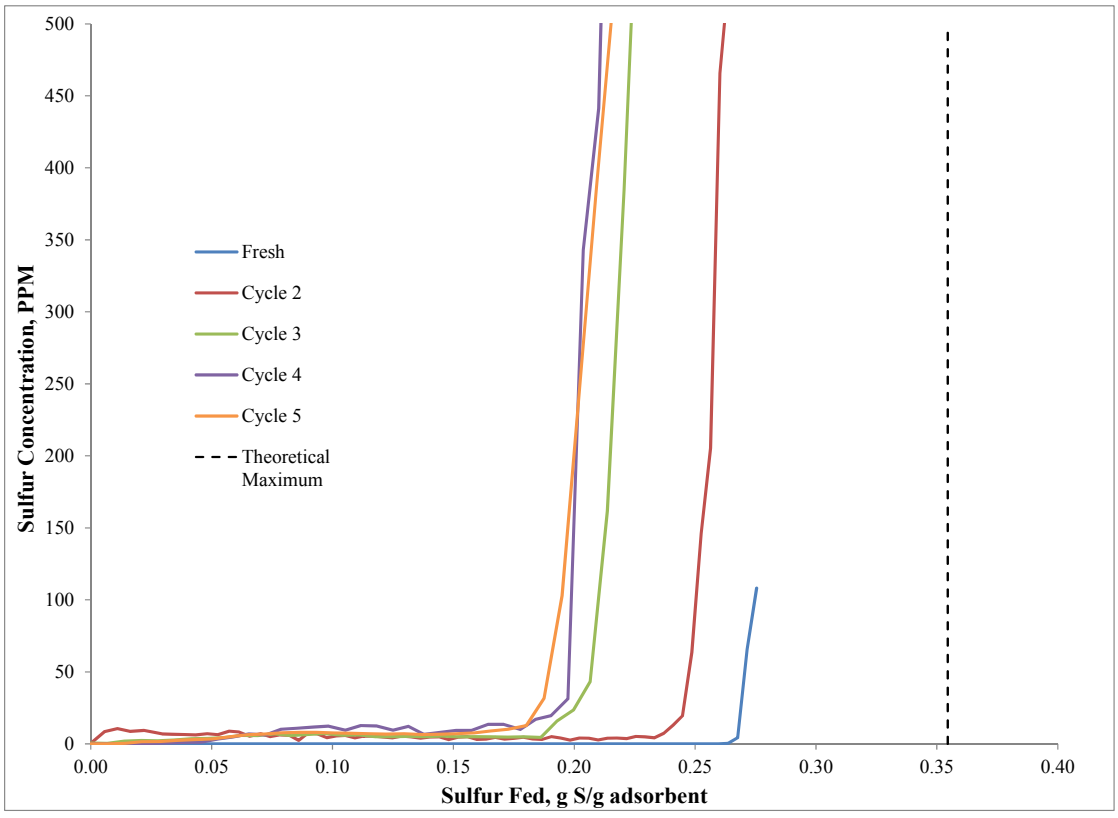

Figure 5.4. Adsorbent Capacity after Multiple Regeneration and Sulfidation Cycles. 3,000 ppm H_2S, sorbent G-72D, Carrier Gas: 38.4% CO, 38.4% H2, 3.2% N2, 20% H_2O, 450ºC, 12,000 $hour^{-1}$ GHSV.

This decrease has been seen in other published data (Tamhankar et al. 1986, Lew et al. 1989). There are many possible causes of a decrease in capacity after the initial sulfidation of the ZnO, including formation of $ZnSO_4$ (Meng et al. 2009), volatilization of zinc (Rosso et al. 2003), and loss of activity of the ZnO (Novochinskii et al. 2004). The increase in sulfur slip concentration after the first adsorption experiment supports a loss in ZnO activity. Volatilization of zinc is thought to be unlikely because the adsorption capacity reached a steady-state value (Rosso et al. 2003). Zinc sulfate, which would be in equilibrium with ZnS (reaction 5.8), might be formed and could cause a steady-state decrease in overall capacity.

$$ZnSO_4 + 2H_2 \leftrightarrow ZnS + 2H_2O \quad (5.8)$$

5.4 Trace Metals Cleanup

Initial screening of potential materials for the removal of trace level inorganic compounds (e.g., AsH_3 and PH_3) stemmed from investigations into alternate candidate materials for sulfur removal. One promising material for adsorption under the conditions of warm syngas cleanup studied was nickel, and as such, it was considered for the removal of other impurities as well. Two primary concerns in the use of nickel were particle sintering and methanation activity. These two effects were respectively lessened by loading and trapping the Ni particles into the cage structure of the SBA-16 and alloying with copper. Nickel and copper also were considered to be promising sorbent materials because downstream synthesis catalysts frequently contain those metals. Thus, contaminants that could poison the downstream catalysts would be trapped by the upstream sacrificial sorbent bed. The combined loading of copper and nickel for this sorbent material was 28.8 wt %, with a copper-to-nickel molar ratio of 1:9. As shown in Figure 5.5 and Figure 5.6, respectively, when using syngas simulant, parts-per-million levels of both PH_3 and AsH_3 were removed to ppb levels (and below our detection limit). Additional results and details are described in previous reports (Li et al. 2009, Howard et al. 2013). It should also be noted that either partial or full thermal decomposition of AsH_3 and PH_3 may occur regardless of sorbent material and is dependent on feed content and process conditions (Howard et al. 2013).

5.5 Conclusions

The total treatment process for warm gas cleanup of inorganics was divided into three major steps: 1) removal of chloride, 2) removal of sulfur, and 3) removal of other trace metal contaminants. Sodium carbonate was found to optimally remove chlorides at an operating temperature of 450ºC. A major impurity of concern in syngas is H_2S. The goal of this study was to determine the effectiveness of commercial ZnO sorbents for removing sulfur from syngas. We were able to show that the optimal sulfur capacity for ZnO occurs at ~450ºC. In addition, the fresh, never-regenerated sorbent was below the target concentration of 100 ppbv at temperatures of 300ºC and 450ºC. We found that sulfur from COS could be adsorbed (to levels below our detection limit of 40 ppb) in the presence of water that leads to no detectable slip of H_2S. In addition, we observed that, even when no water is in the feed and the temperature is 450ºC, COS is able to react with ZnO, and there is no measureable sulfur slip.

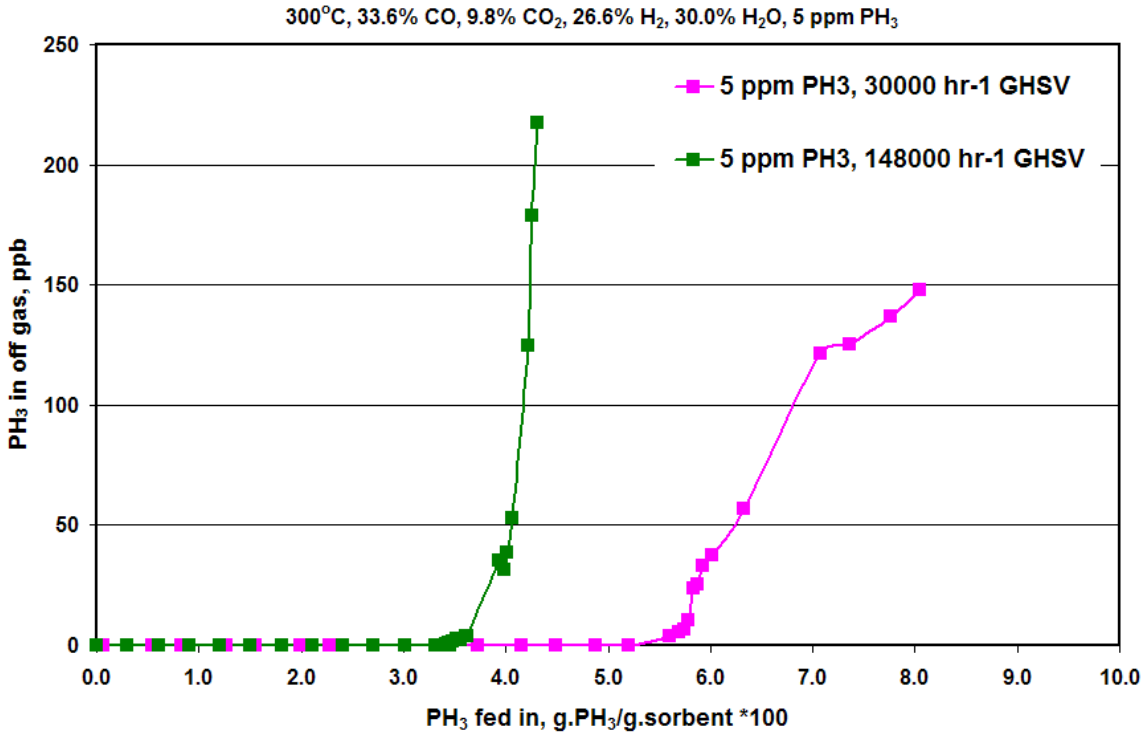

Figure 5.5. PH_3 Adsorption using Cu-Ni/SBA-16 (300°C and GHSV = 30,000 hr^{-1} or 148,000 hr^{-1}; Feed composition: 30.0% H_2O, 33.6% CO, 9.8 CO_2, and 26.6% H_2, 5 ppm PH_3).

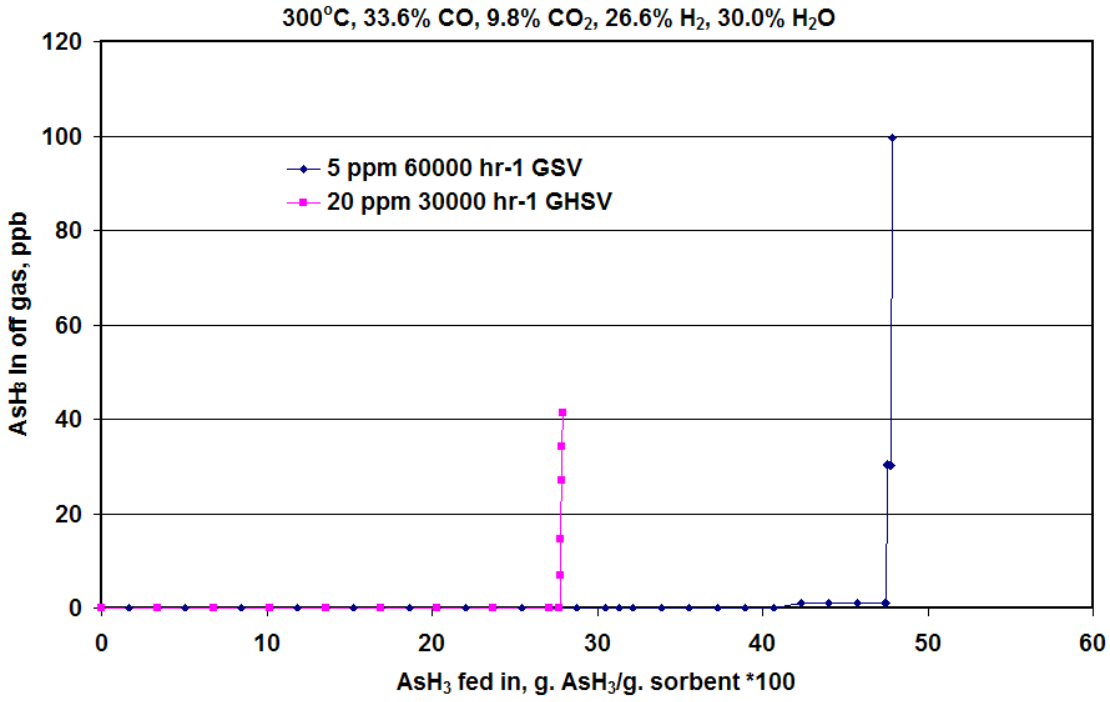

Figure 5.6. Warm AsH_3 Adsorption using Cu-Ni/SBA-16 (300°C and GHSV = 30,000 hr^{-1} or 60,000 hr^{-1}; Feed composition: 30.0% H_2O, 33.6% CO, 9.8 CO_2, and 26.6% H_2, and 5 or 10 ppm AsH_3).

Our experiments with regeneration of the ZnO sorbent indicate that there is some capacity loss associated with repeated regeneration of the material; however, the capacity is mostly stable after two to three regenerations. We did observe an appreciable slip of H_2S (5 to 10 ppm) from the regenerated ZnO to concentrations that were above levels predicted by thermodynamic equilibrium. This increased slip may be related to a loss in ZnO surface activity after regeneration. Similar to capacity, this loss reached a plateau after several (i.e., two to three) regenerations.

Finally, a sorbent material containing both copper and nickel was found to be effective in removing trace metal impurities such as AsH_3 and PH_3 when operating at 300ºC.

6.0 Integrated Process Demonstration of Coal-Derived Warm Syngas Cleanup

6.1 Introduction

Generating low-CO_2 SNG from coal gasifier-derived syngas using warm cleanup requires many unit operations. In previous work pertaining to warm cleanup of biomass-derived syngas, we identified contaminants requiring removal, including alkali salts, chloride, sulfur compounds, heavy metals, ammonia, and various compounds containing potassium, arsenic, antimony, and selenium (Howard et al. 2013). Similar contaminant species are present in coal-derived syngas. In this chapter, we describe a bench-scale demonstration for the integrated process and materials developed in this study.

The dry composition of the syngas used in this study is shown in Table 6.1 and Table 6.2. The syngas was generated by the Western Research Institute in Laramie, Wyoming, using Decker coal. Prior to bottling, the syngas was condensed out. The measured contaminants of the resulting dried syngas are reported in Table 6.1. It should be noted that some of the contaminants initially present in the syngas were removed out in the condensation. It is envisioned that actual implementation of this warm cleanup approach would likely not include water quenching, which is deleterious to process thermal efficiency. Thus, impurities would be greater in concentration if a water quench was not employed. For comparison, in Table 6.2 the potential expected ranges of contaminants also are shown. Based on our experience, this is an estimate for the quantities that would be expected to be present in the raw syngas prior to condensation. Water was thus added to the syngas using a microchannel vaporizer before being fed to the process. Experimental methods are described in more detail in our previous report (Howard et al. 2013).

Table 6.1. Wyoming Coal-Derived Syngas Composition (mol%).

	H_2	N_2	CO	CO_2	CH_4	C_2H_4	C_2H_6	C_3H_8	H_2O
Dry	48.84%	1.38%	35.29%	13.44%	0.87%	0.13%	0.04%	0.01%	N/A
Wet	39.07%	1.10%	28.23%	10.75%	0.70%	0.10%	0.03%	0.01%	20.00%

Table 6.2. Coal-Derived Syngas Contaminants

Contaminant	H_2S	COS	NH_3	HCN	HCl	AsH_3
Measured (ppm)	290	<2 ppmv	75	18	N/A	N/A
Potential (ppm)	500–1,000	20–30	1,500–3,000	50–70	25–100	3–10

6.2 Process Description

A block flow diagram of our process is shown below in Figure 6.1. There are six general unit operations used to treat the syngas and generate the desired products. A complete breakdown of these unit operations and their catalysts is in Table 6.3.

The first unit operation, R1, is for the removal of any chloride present in the syngas. Chloride in the form of HCl can be present in syngas from the gasification of coal (Cayan et al. 2008) and biomass (Torres et al. 2007). Hydrogen chloride can be removed from the process stream by reaction within a

fixed bed or alkaline material, such as $CaCO_3$ or Na_2CO_3 (Verdone and De Filippis 2006). In this study we used sodium carbonate because of its high efficiency as described in Chapter 5. This bed was operated at a temperature of 450ºC.

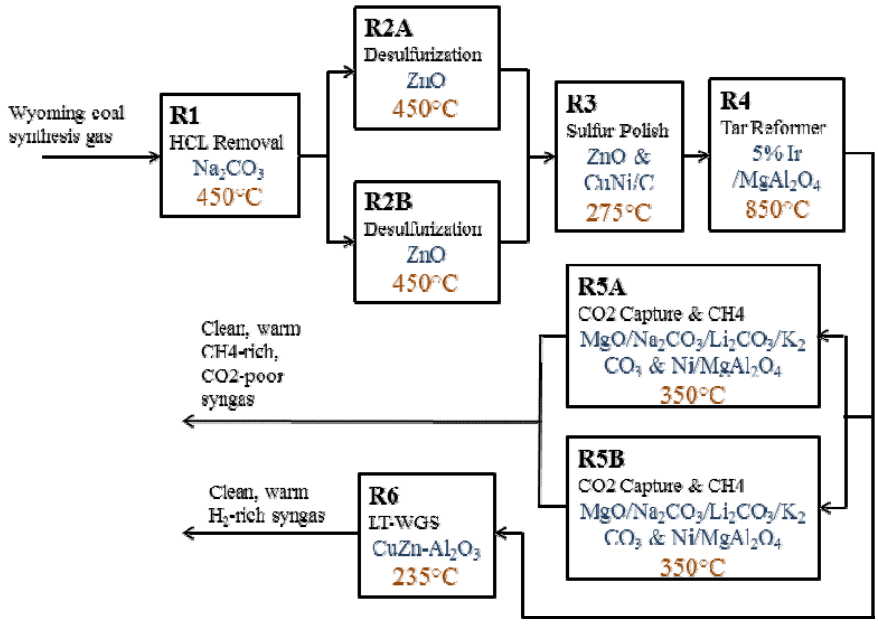

Figure 6.1. Block Flow Diagram of Warm Syngas Cleanup Process

Table 6.3. Reactor Loadings

			Particle Size		Mass
Reactor	Material	Source	(mesh #)	(μm)	(g)
R1	Na_2CO_3	Sigma-Aldrich	30–60	250–595	21.6
R2A	ZnO, Actisorb S2	Süd-Chemie	30–60	250–595	30.6
R2B	ZnO, Actisorb S2	Süd-Chemie	30–60	250–595	36.9
R3	ZnO, Actisorb S3	Süd-Chemie	60–80	177–250	13.8
	ZnO, Actisorb S2	Süd-Chemie	60–80	177–250	10.5
	Cu-Ni/C	PNNL	30–60	250–595	2.5
R4	5% Ir/$MgAl_2O_4$	PNNL	60–100	149–250	0.25
	Al_2O_3	Alfa Aesar	60–100	149–250	2.5
R5A	30% Ni/$MgAl_2O_4$	PNNL	60–80	177–250	0.67
	$MgO/Na_2CO_3/Li_2CO_3/K_2CO_3$	PNNL	40–60	250–400	10
	SiC	Atlantic Equipment Engineers	60–80	177–250	3.33
R5B	30% Ni/$MgAl_2O_4$	PNNL	60–80	177–250	0.68
	$MgO/Na_2CO_3/Li_2CO_3/K_2CO_3$	PNNL	40–60	250–400	10
	SiC	Atlantic Equipment Engineers	60–80	177–250	3.38
R6	Cu-Zn/Al_2O_3	Alfa Aesar	60–100	149–250	4
	Al_2O_3	Alfa Aesar	60–100	149–250	12

The second unit operation, R2, is broken up between two regenerable beds of ZnO for the bulk removal of sulfur. Based on previous experience (Howard et al. 2013) and recent work with warm sulfur adsorption, we operated these beds at 450ºC. The regeneration was carried out at 650ºC with 5% O_2 in N_2 while the alternate reactor was in line with the system.

We expect a slip of sulfur from the bulk sulfur operation in the range of 1 to 5 ppmv H_2S. To remove this sulfur we use a non-regenerable sulfur polishing bed, R3. The bed is made up of ZnO operating at a lower temperature than the bulk removal to take advantage of the improved slip thermodynamics as well as a copper/nickel/carbon sorbent after the ZnO to remove any sulfur that does bypass the ZnO. Because of the adsorption temperature requirements of the copper/nickel/carbon sorbent the sulfur polish bed was operated at 275ºC (Rostrup-Nielsen and Pedersen 2010). This copper/nickel/carbon sorbent was also used to remove a multitude of metal contaminants. It should be noted that this material was used in lieu of the copper/nickel/SBA-16 sorbent as described in Chapter 5 because of the cost of the SBA-16 material. Using a carbon-based support would be a cheaper alternative and, thus, was investigated further.

The gasifier that produced the raw syngas used for this demonstration was operated at a lower temperature (~900ºC) than would be expected for commercial-scale gasification. Thus, from prior experience, this syngas contains the presence of larger hydrocarbons materials and tars (i.e., polyaromatic hydrocarbons) that could lead to carbon deposition on downstream catalysts. For this reason, to steam reform these compounds, a high-temperature tar reformer was placed after the sulfur removal unit operations, R4. Such a tar-reforming unit was used for the case of warm cleanup of biomass-derived syngas (Howard et al. 2013). This catalyst also was been shown to be active for ammonia decomposition (Howard et al. 2013). It is anticipated that, in a real application involving coal-derived syngas, the gasifier would be operated at temperatures high enough to prevent the formation of tars, thus a tar-reforming unit would not be necessary.

The overall objective of high carbon selectivity toward SNG with CO_2 capture is accomplished in the fifth unit operation, R5. However, because of the current state of carbon capture technology, the system flow rates of 1 L/min of syngas were impractical. To test the viability of this unit operation, the R5 unit operation was fed a slip stream of about 5 sccm of the process gas exiting R4. There were two R5 beds to allow regeneration of the CO_2 capture material. The operation was performed at 350ºC, and regeneration under a N_2 atmosphere occurred at 450ºC.

To demonstrate the efficiency of the cleanup portion of the process, most of the syngas was sent to a low-temperature WGS catalyst. Copper-based catalysts are known to be very susceptible to catalyst poisons. Thus, monitoring WGS activity of this catalyst would offer secondary indication of inorganic contaminant removal efficiency. This commercial $Cu/ZnO/Al_2O_3$ catalyst was operated at 235ºC for 100 hours time-on-stream.

6.3 100-Hour Process Demonstration

The integrated process (Figure 6.1) was operated continuously for 100 hours with approximately 1 SLPM of raw syngas feed. Catalytic performance results for the WGS catalyst, R6, are shown in Figure 6.2. No noticeable decrease in CO conversion was observed, within statistical measure. No H_2S—or any other gaseous contaminant—was observed in the outlet. The lower limit for sulfur detection

is 40 ppb. It should be noted that postmortem analysis of the WGS catalyst (results shown below) revealed ppm levels of sulfur on the front end of the catalyst bed, whereas the back end of the bed remained sulfur-free. Thus, it appears that small amounts of sulfur—likely parts per billion levels—slipped past the sulfur and trace metal guard beds and accumulated on the front end of the WGS catalyst bed. Regardless, these results were very promising and offer significant progress compared to past demonstrations.

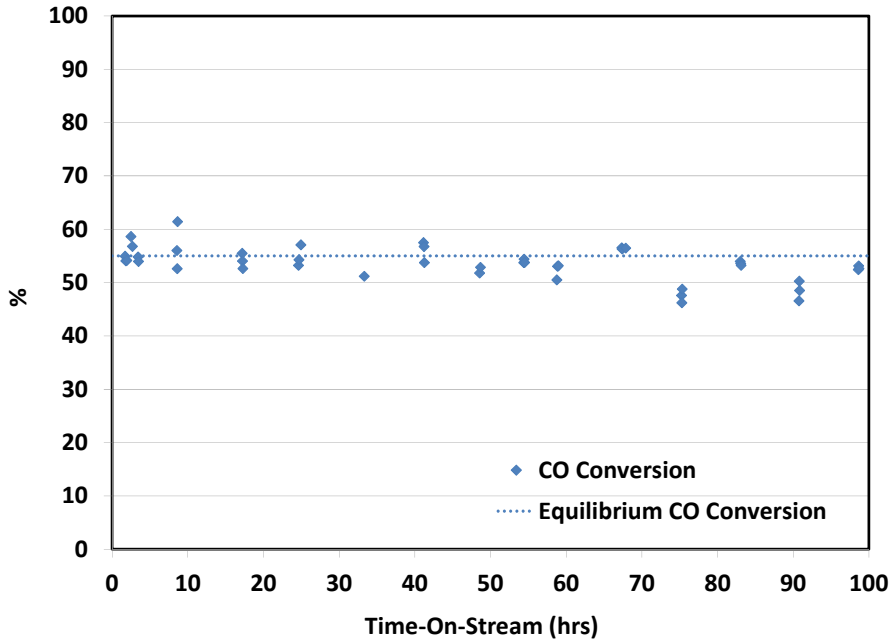

Figure 6.2. WGS Catalyst (R6) Performance during Continuous 100-Hour Demonstration of the Warm Cleanup Process

For the sorption-enhanced methanation beds, R5, only a 3 to 10 sccm slipstream was used for demonstration. Over the course of the experiment the R5A reactor showed a general decline in its CO conversion, Figure 6.3. For the same tests, the efficiency of the CO_2 capture material was more sporadic. The amount of CO_2 captured ranged from 30 to 80% for R5A over the course of the 100-hour test.

With the exception of one test period during the experiment, R5B had a complete loss in capture ability for its CO_2 capture material (data not shown). The cause of loss is unclear because there was no experimental difference between the two beds (R5A vs. R5B). Furthermore, postmortem analysis does not support a poisoning hypothesis. It is known that the CO_2 capture material is sensitive to impurities and also has a small temperature window of operation. Further study is needed to fully understand the deactivation mechanism for the integrated bed.

Further enhancement to CO_2 sorption and, thus, an increase in gas phase CH_4 selectivity could occur if the system were operated at elevated pressure. Unfortunately, for the 100 hour demonstration, we were unable to operate at elevated pressure because of the low supply pressure of the syngas cylinders. However, we were able to demonstrate the advantage of pressure with tests on the CO_2 sorbent and methanation catalyst using model syngas simulant (as reported in Chapter 4.0). In these tests >99% conversion of CO was achieved with near complete CO_2 capture. Thus, applicability for this process under pressurized conditions has certainly been realized.

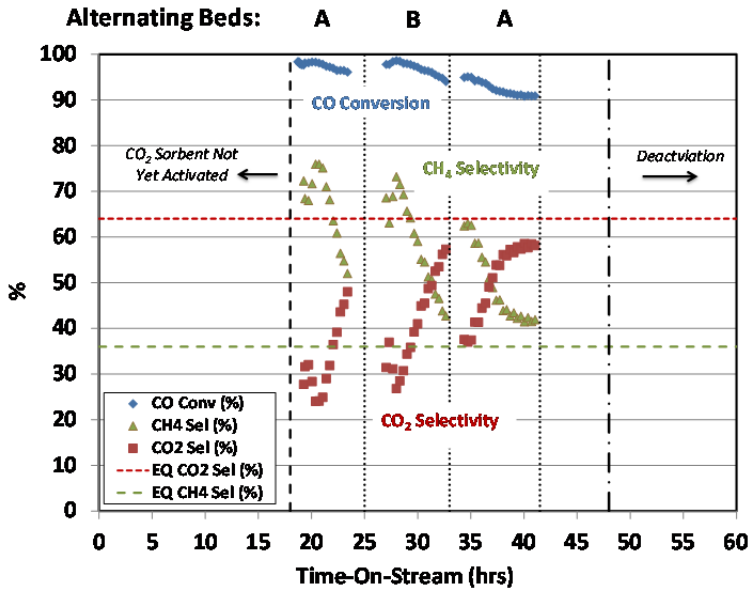

Figure 6.3. Initial Performance of the R5A and R5B Carbon Dioxide Capture and Methanation Integrated-Bed Reactor. The calculated gas phase equilibrium product selectivities assume no CO_2 capture.

6.4 Postmortem Catalyst and Sorbent Characterization

For postmortem analysis reactor beds were typically divided into five equal sections. The first section, R-1, indicates the inlet of the bed, R-3, is the middle section of the bed, and the final section, R-5, indicates the outlet. The reactor beds were analyzed for sulfur and arsenic using inductively coupled plasma and sulfur, chloride, and nitrate using ion chromatography, Table 6.4. Unlike our previous work there was no detectable arsenic in any of the reactor beds tested (Howard et al. 2013). Because of size constraints, R3 and R4 were not sectioned into five parts.

6.4.1 Chloride and Nitrate Removal, R1

Ion chromatography results for the Na_2CO_3 bed indicate a slight adsorption of sulfur in the form of sulfate, and trace adsorption of chloride and nitrates. There is a dramatic decrease in the chloride collected on R1 compared with our previous work (Howard et al. 2013). This is likely due to a lower concentration of chlorine in the real syngas than we had modeled before and not any difference in the effectiveness of the reactor bed.

Table 6.4. Ion Chromatography and Inductively Coupled Plasma (ICP) Results

	R-1			R-2A (after sulfidation)		R-2B (after regeneration)		R-3 ZnO		R-3 NiCu/C		R-4		R-5A		R-5B		R-6	
Analyte (ppm)	Sulfur	Chloride	Nitrate	Sulfur	Arsenic	Sulfur	Arsenic	Sulfur	Arsenic	Sulfur	Arsenic	Sulfur	Arsenic	Sulfur	Arsenic	Sulfur	Arsenic	Sulfur	Arsenic
Fresh	102	0	0	778	<20	778	<20		<20		<35	--	--	--	--	--	--	--	--
Inlet	462	12	31	187,300	<30	224,400	<20	750	<20	222.7	<35	<20	<40	98	<20	34	<20	13,490	<40
Middle	107	15	48	699	<20	1,142	<20	--	--	--	--	--	--	--	--	--	--	<40	<40
Outlet	97	8.3	31	821	<20	845	<20	595	<20	--	--	--	--	<20	<20	42	<20	<40	<40

6.4.2 Bulk Sulfur Removal, R2A & R2B

The XRD patterns for sections from R2A and R2B shown in Figure 6.4 R2A were taken from the reactor after sulfidation and R2B after regeneration. The X-ray diffraction results indicate clear uptake of sulfur by the ZnO. The existence of ZnS in the XRD patterns supports sulfur removal by adsorption on the ZnO support (see reaction 6.1).

$$H_2S + ZnO \rightarrow H_2O + ZnS \qquad (6.1)$$

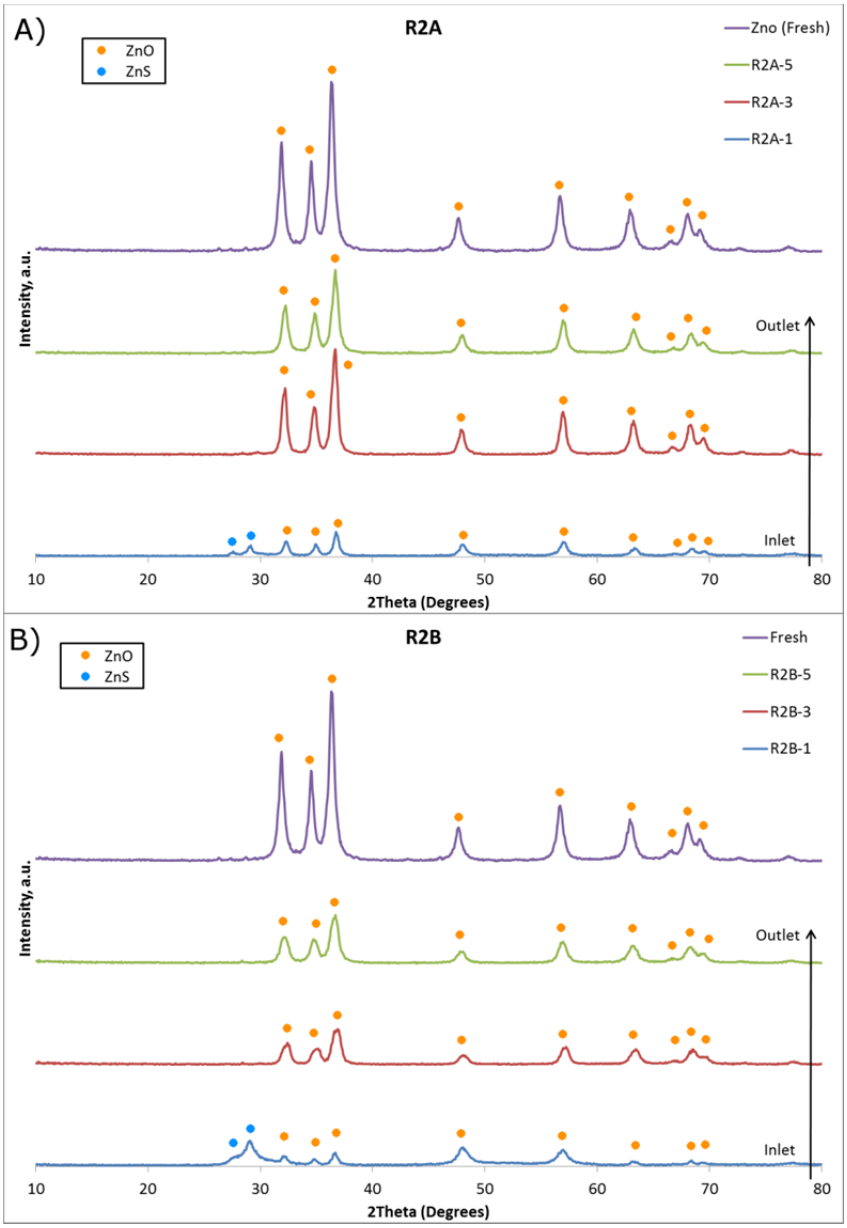

Figure 6.4. XRD Patterns for R2A (A) and R2B (B), ZnO for Bulk Sulfur Removal Reactors. R2A reactor is after sulfidation, and R2B is after regeneration.

The sulfur is mostly located in the first section of both reactor beds. This indicates that the majority of the sulfur was captured at the front end of the bed. This result is supported by the ICP data as shown in Table 6.4. The sulfided bed (187,300 ppm sulfur) and regenerated bed (224,400 ppm sulfur), R2A and R2B, respectively, both contain significant concentrations of sulfur on the front end of the bed as evidenced by ICP (Table 6.4). The middle and outlet of both beds contain lesser amounts of sulfur. Thus, the sulfided bed was not completely sulfided. Zinc oxide and ZnS crystal size data for both spent sorbents are shown in Table 6.5.

Table 6.5. Mean Crystal Size Estimated From the Scherrer Equation

	Mean Crystal Size, nm			
	R2A (after sulfidation)		R2B (after regeneration)	
	ZnO	ZnS	ZnO	ZnS
Fresh	3.347	-	3.347	-
Inlet	3.567	97.37	3.273	46.22
Middle	3.136	-	2.062	-
Outlet	3.029	-	2.332	-

The result that the ZnO bed was not able to fully regenerate is different than we had previously observed and reported (Howard et al. 2013). Possible reasons for this diverging result include the fact that the current study used 1) a different commercial ZnO sorbent material, 2) a lower H_2S feed concentration, and 3) real syngas, whereas a simulated syngas was used in the previous study. As noted before in our baseline sulfur tests, the new sorbent used in this study exhibited a decrease in sulfur capacity compared to the previously used sorbent (Howard et al. 2013). However, the new sorbent did show a similar resiliency to regeneration and sulfur slip.

6.4.3 Sulfur Polish, R3

The sulfur polish bed was made up of two different materials: ZnO and Cu-Ni/C. The Cu-Ni/C sorbent was also used for trace removal of other metal contaminants. ICP analysis for both the ZnO and Cu-Ni/C spent materials indicate relatively low sulfur adsorption. Although it should be noted that sulfur capacity for this particular Cu-Ni/C material is unknown. The presence of sulfur downstream of the R3 bed indicates incomplete sulfur sorption. The combined bed temperature was lower than we had used in our previous work (~250 vs. 300ºC). Thus, decreased kinetics could explain its lower effectiveness (Howard et al. 2013). Nonetheless, the vast majority of sulfur was removed in the ZnO beds thus providing proof-of-concept for this segment of the process.

6.4.4 Tar Reformer, R4

The XRD patterns for R4 (not presented here) do not reveal the presence of any contaminant species or metal sintering. This finding is confirmed by ICP results that do not reveal the presence of sulfur. Additionally, total carbon analysis indicates no carbon fouling. The absence of sulfur can likely be attributed to the relatively high operating temperature (850ºC); a temperature regime in which sulfur sorption is not favored. However, sulfur is present downstream of the tar-reforming catalyst. The

absence of sulfur and carbon found in the tar-reforming bed is an improvement over our previous results where low levels of both carbon and sulfur were observed. The previous results may have also been related to the relatively high concentrations of tars that were introduced to the system (Howard et al. 2013).

6.4.5 Methanation and Carbon Dioxide Capture, R5A and R5B

The postmortem analysis of R5 by ICP and total carbon analysis, Table 6.6, indicate the presence of sulfur and carbon formation in the entry portions of both reactors. However the presence of these contaminants cannot explain the losses that occurred on R5B. The carbon formation observed on R5A may be responsible for the decrease in CO conversion observed in the experiment.

Table 6.6. Total Carbon Analysis of the Carbon Capture Beds

	Wt% Carbon	
	R5A	R5B
Fresh	0.367	0.367
Inlet	9.752	3.246
Outlet	1.953	0.936

The XRD results for R5A and R5B (Figure 6.5) do not show the presence of any peaks that were not present in the fresh sample. However, both front-end regions show dramatically decreased peak sizes that can be correlated with loss of crystallinity of the material. While sulfur and carbon are not detected in these front-end regions, they may be responsible for the loss of crystallinity of the material. However, temperature gradients as cause for loss of sorbent material effectiveness cannot be ruled out.

6.4.6 Water-Gas-Shift, R6

The ICP results for the WGS catalyst bed indicate the presence of sulfur in the first section of the bed (Table 6.4) with no measurable amount of sulfur present in the middle and outlet sections. This catalyst was chosen for our demonstration because it is highly susceptible to sulfur contamination; therefore, it is not completely surprising that some sulfur slipped through the bulk sulfur and sulfur polish beds. The total carbon analysis of the WGS bed indicates the presence of carbon deposits (Table 6.7).

The conditions of the experiment put the WGS bed in a regime that was limited thermodynamically rather than kinetically so the loss of any catalyst surface area was not noticeable. In a separate experiment, the spent WGS catalyst was compared to fresh catalyst in a kinetically limiting regime. The impact of the carbon formation and sulfur on the catalytic performance of the WGS catalyst can be seen in Figure 6.6. The consistent slight decrease in CO conversion activity indicates that, over the course of the 100 hour test, there was some poisoning of the catalyst. However, this loss in activity was minimal, suggesting that there was only very minimal deactivation of the catalyst after 100 hours of time-on-steam. Thus, the raw syngas is significantly purified in the warm cleanup process.

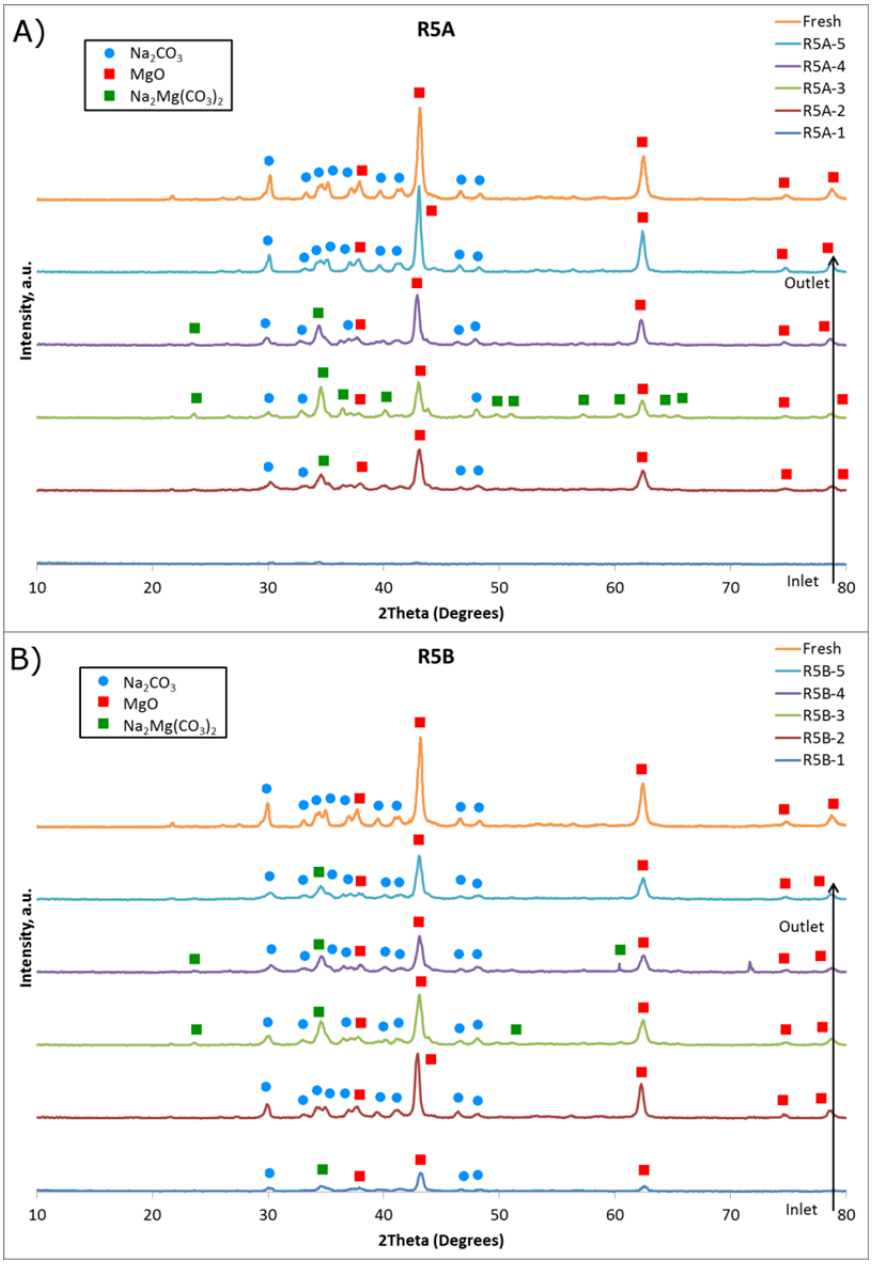

Figure 6.5. XRD Patterns for the R5A (A) and R5B (B) Carbon Dioxide Capture and Methanation Reactors. R5A reactor is after process, and R2B is after regeneration.

Table 6.7. Total Carbon Analysis of the WGS Bed

	R6-1	R6-2	R6-3	R6-4	R6-5
Carbon, wt %	0.197	0.133	0.126	0.170	0.207

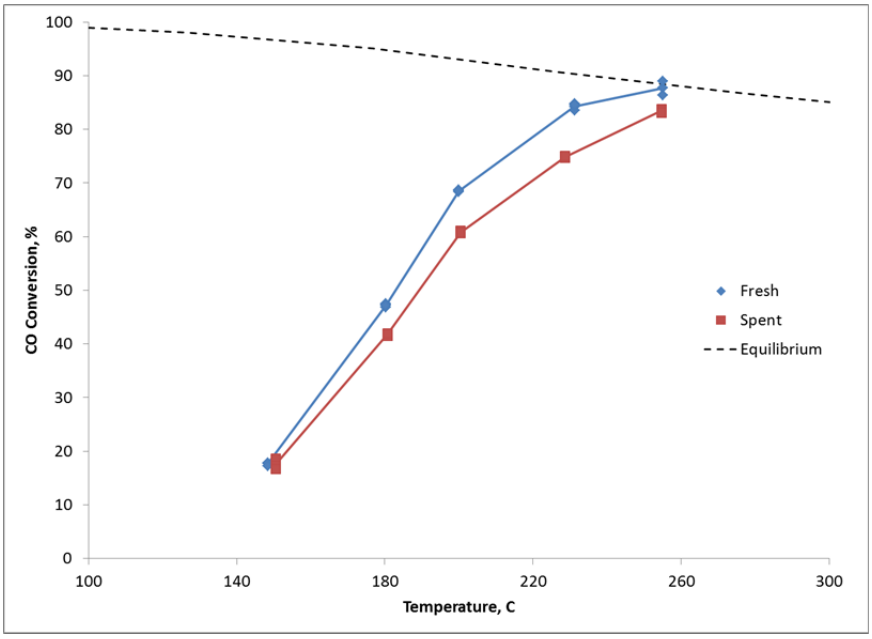

Figure 6.6. Activity testing of the $Cu/ZnO/Al_2O_3$ WGS Catalyst (38.4% H_2, 38.4% CO, 3.2% N_2, 20% H_2O, 46,000 hr^{-1} GHSV, atmospheric pressure)

6.5 Conclusions

In this study, we successfully demonstrated the potential for a process enabling CO_2 sorption-enhanced SNG production, generated from coal-derived syngas using warm cleanup. The SNG and CO_2 capture bed R5A provided initial proof-of-concept for a combined capture and methanation reaction, albeit degraded sorbent efficiency was observed. The high methane selectivity observed, approaching 80%, is very promising. The reason for the poor performance of the second SNG and CO_2 capture bed, R5B, is not completely understood. Postmortem analysis of the R5 unit operation does not suggest sulfur as the cause of the for performance loss. However, carbon formation was observed. In addition, XRD analysis reveals loss of sorbent crystallinity.

Based on the WGS catalyst postmortem analysis and by evaluating catalytic performance before and after the 100 hour demonstration, we found that the vast majority of impurities were removed from the raw syngas. However, a slight decrease in WGS activity did occur. Postmortem analysis as evidenced by ICP revealed the presence of parts-per-million levels of sulfur on the front end of the WGS bed. The slight drop in activity of the WGS catalytic performance is attributed to sulfur poisoning. The sulfur polishing bed failed to capture *all* of the sulfur that was slipping through the sulfur bulk unit operation. Further optimization of this unit operation is needed to completely protect downstream synthesis catalysts. Regardless, the vast majority of poisons were removed from the raw syngas proving the viability of the warm cleanup process.

7.0 Preliminary Technoeconomic Analysis

To compare the laboratory-developed syngas cleanup technologies to conventional coal cleanup technologies, two coal gasified syngas cleanup processes are simulated and evaluated in this study. Cold syngas cleanup technologies have been conventionally used in coal gasification plants. Recently, warm syngas cleanup technologies have been under development. The advantages for a warm or hot syngas cleanup process include eliminating the need to cool the syngas and increasing heat recovery.

For the technoeconomic analysis H_2 was the target product (instead of SNG). A process and economics for a "conventional" cold cleanup case was compared to that of a warm cleanup approach designed for hydrogen production. While the warm cleanup approach used for this case does not include CO_2-sorption assisted methanation, as described earlier in this report, it does utilize the double salt sorbent technology which is extended to CO_2-soprtion assisted water-gas-shift.

7.1 Process Description

The feedstock used in this study is raw syngas from coal gasification. The raw syngas conditions and compositions are listed in Table 7.1. The same feedstock and product of pure H_2 were assumed for both processes.

Table 7.1. Raw Syngas Specifications

Feedstock	Raw Syngas from Coal Gasification
Temperature, ^oF	1,250
Pressure, psia	805
Composition, wt%	
Nitrogen	1.85%
Fly ash	1.66%
Hydrogen	4.72%
Carbon Monoxide	47.34%
Carbon Dioxide	28.27%
Methane	0.67%
Ethene	0.17%
Ethane	0.051%
Propane	0.025%
Water	14.75%
Ammonia	0.29%
Carbonyl Sulfide	0.0068%
Hydrogen Sulfide	0.19%
Hydrogen Chloride	0.0021%
HCN	0.011%

7.2 Cold Syngas Cleanup Process

A simplified process flow diagram for a cold syngas cleanup process is shown in Figure 7.1(a). In this process, raw coal syngas from a gasifier is water quenched and then scrubbed to remove most of the particulate matter (PM) and trace impurities such as ammonia and hydrogen chlorides. The PM-free syngas is then sent to a two-stage sour shift reactor. The CO conversion efficiency is assumed to be ~97%. Most of the COS is converted to H_2S. Then, carbon beds are used to remove mercury from the

shifted gas. The spent carbon is disposed of as solid waste. The syngas is sent to a two-stage acid gas removal (AGR) unit (Selexol) to remove over 99% of the H_2S and 90% of the CO_2. The acid gas is fed to a sulfur plant to produce elemental sulfur. The tail-gas is further treated, and the off gas is recycled to the Selexol process. The sulfur removal requirement for this process is at the extreme limit of Selexol's capabilities. To guarantee over 99.99% removal efficiency regardless of fluctuations in coal sulfur content or system performance, a ZnO guard bed was used after the Selexol process to remove trace sulfur contaminants. The low-temperature syngas from the Selexol process is heated and then fed to the ZnO bed. The syngas is cooled and then sent to a pressure swing adsorption (PSA) unit to produce purified H_2. The remaining syngas is burned in a furnace for heat recovery to generate steam for power generation. The major pollutant control methods and control targets assumed in this study are listed in Table 7.2.

7.3 Warm Syngas Cleanup Process

The process diagram for the warm gas cleanup process is shown in Figure 7.1(b). In this process, raw coal syngas is sent to cyclones and candle filters to remove fine PM. Then, Na_2CO_3 absorbent is used to remove HCl from the syngas. The syngas is sent to a transport ZnO bed for sulfur bulk removal. The sulfur content in syngas can be reduced to <5 ppm. The spent absorbent is regenerated by air, and the regenerated catalyst is recycled to the absorption bed. Sulfur dioxide generated during regeneration is used to produce sulfuric acid as a byproduct. Almost all the sulfur then is removed from the syngas in a sulfur polish bed using ZnO as the absorbent. When spent, the absorbent is disposed of as solid waste. The sulfur-free syngas is then sent to a trace metal removal unit to remove most trace metals, such as arsenic and lead. The syngas is fed to a mixed water-gas shift and CO_2 removal process to convert about 99% CO to CO_2 and absorb about 90% CO_2 at the same time. The spent absorbent and catalyst is regenerated using hot N_2, which is assumed to be from an air separation unit in a coal gasification system and, therefore, is readily available for use in this process. The N_2 from the air separation unit is heated by fuel gas combustion and then fed into the catalyst bed. Carbon dioxide is desorbed and mixed with N_2. This mixture is cooled by steam generation and then assumed to be released to the atmosphere. The cleaned syngas also is cooled by boiler feed water and then cooling water. The cooled syngas is used to generate purified H_2 by a PSA unit. The off gas is used as fuel gas for catalyst regeneration and steam generation. Table 7.2 lists the major pollutants control methods and control targets assumed in this study.

7.4 Evaluation Method

Process models for both cold and warm syngas cleanup processes are developed in ChemCad, which is a chemical process steady-state simulator. The design of cold syngas cleanup process is based on information published in the literature (Black 2010, Spath et al. 2005). The design of the warm syngas cleanup process is based on data obtained from laboratory testing. Cost estimates are based on information from the literature and cost estimating software. Estimates of the cost of major equipment in the cold syngas cleanup process are based on cost information published by Black (2010) and Spath et al. (2005) and are scaled based on process simulation results. The process simulation results, primarily including flowrates, heat duty, power generation, and stream conditions, were used to estimate the size of the equipment or for scaling the base cost. The costs of major equipment in the warm syngas cleanup process were estimated by inputting the size information to the Aspen Process Economic Analyzer and. Cost estimates for some special equipment, such as the candle filter, sulfuric acid plant, and PSA, are based on data from the literature (Craig and Mann 1996, NETL 2000, Spath et al. 2005).

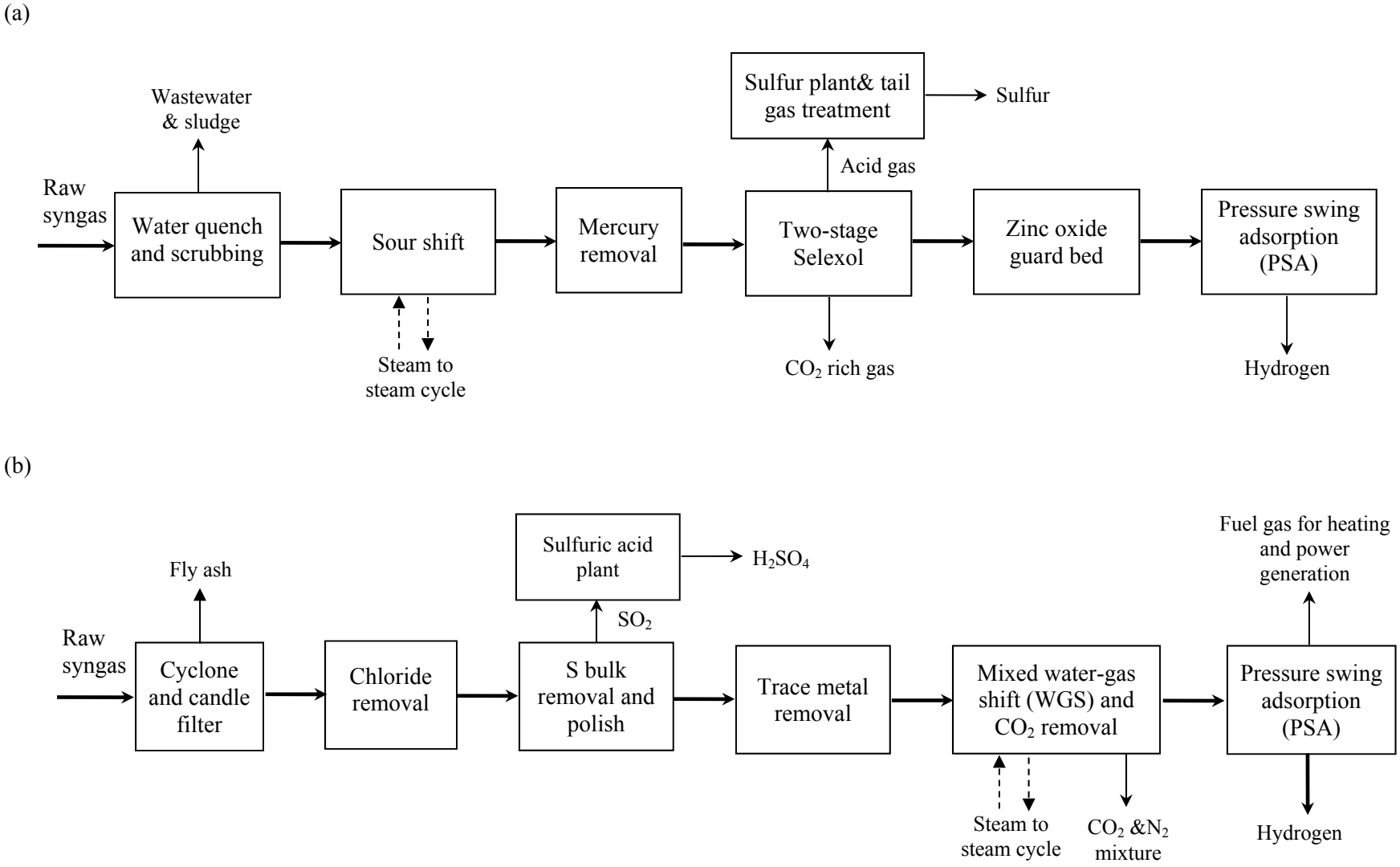

Figure 7.1. Simplified Process Flowsheet for (a) Cold Gas Cleanup Process; and (b) Warm/Hot Gas Cleanup Process for Coal Gasification to Methanol Synthesis System

Table 7.2. Summary of Major Pollutants, Control Methods, and Targets

Major Pollutants	Cold Gas Cleanup	Warm Gas Cleanup
PM	Quench and wet scrubbing	Cyclone and candle filter
Chloride removal	Quench and wet scrubbing	Dry absorption by Na_2CO_3
SO_2	Two-stage Selexol	ZnO bed for S bulk removal
Sulfur polish	ZnO guard bed	ZnO bed
Sulfur recovery	Sulfur plant	Sulfuric acid plant
CO_2	Two-stage sour shift reactors and two-stage Selexol	Mixed WGS and CO_2 absorption unit
Trace metal removal	Mercury removal by carbon bed	As/Pb removal by Cu-Ni/AC adsorption
Pollutant Removal Target	**Cold Gas Cleanup**	**Warm Gas Cleanup**
CO conversion	97%	99%
CO_2 removal	90%	90%
Sulfur removal	>99.99%	>99.99%
PM	>99.9%	>99.9%

The detailed specifications for the warm gas cleanup technologies are listed in Table 7.3.

Table 7.3. Major Specifications for Warm Gas Cleanup Technologies

Processes	Units	Cl Removal	S Bulk Removal	S Polish	Trace Metal	Mixed Shift and CO_2 Removal
Operating pressure	psia	850	850	850	850	850
Operating temperature	F	450	450	300	300	360
Process pressure drop	psi	10	10	10	10	30
GHSV	$hour^{-1}$	7,000	7,000	7,000	7,000	1,000
Regeneration media and conditions		n/a	Air, 650°C	n/a	n/a	N_2, 400 to 600°C
Regeneration, time	hours	n/a	8	n/a	n/a	0.5 hour
Sorbent/catalyst		Na_2CO_3	ZnO	ZnO	Cu-Ni/AC	MgO +20% $LiNaKCO_3$
Sorbent bulk density (in cart)	lb/ft3	62	70	70	62	62
Pollutant target		chloride	sulfur	sulfur	As/Pb	CO, CO_2
Pollutants uptaking capacity	wt%	33	25	25	5	50
Pollutants control target		<1 ppm	5 ppm	< 60 ppb	< 1ppm	CO conversion 99%; CO_2 removal 90%
Sorbent life	yrs	2	5	5	5	2
Sorbent price, 2011 USD	$/lb	$10	$7.40	$7.40	$35	$15

7.5 Results and Analysis

The major performance results are listed in Table 7.4. The cold gas cleanup process has about 3% lower H_2 generation because of the slightly lower CO conversion efficiency assumed for the sour shift reactors in the coal gas cleanup, which achieves 97% CO conversion. We assumed 99% CO conversion in the mixed shift and CO_2 removal unit in the cold gas cleanup process. A significant amount of sensible heat in the hot streams of the cold syngas cleanup process is lost during water quenching and scrubbing. In addition, the low operating temperature leads to heat loss to cooling water. The warm gas cleanup process operates at medium to high temperatures so much less heat is lost to cooling water. Therefore, more sensible heat is recovered and used for power generation. The cold syngas cleanup process also consumes power for AGR or for the Selexol process. Therefore, the net power generation for the cold process is much lower than that for the warm process. Because it operates at low temperature and thus provides less heat for steam generation, the cold gas cleanup process has a higher cooling-water makeup requirement and a lower boiler feed-water makeup requirement.

Wastewater discharges from the cold syngas cleanup process are lower than those from the warm cleanup process because some of the wastewater is recycled for water quenching and scrubbing. Using water quenching and scrubbing increases the moisture content in the syngas so less steam is used for the shift reaction. In contrast, the warm syngas process consumes more steam for the shift reaction. The amount of spent trace metal adsorbent from the cold syngas cleanup process is much lower than that from the warm gas cleanup process because a large amount of trace metals are assumed to be removed by water quenching and scrubbing. Only mercury needs to be removed by carbon beds. In the warm syngas cleanup process, the dry PM removal process is not effective for removing trace metals that are present in vapor phase under high temperature. Therefore, the load on the trace metal removal unit in the warm cleanup process is large, and the amount of the spent catalyst is higher than that for the catalyst used for mercury removal in the cold syngas cleanup process.

More CO_2 is captured in the warm syngas cleanup process than in the cold cleanup process because of the higher CO conversion in the mixed WGS and CO_2 process. Nitrogen oxide emissions in the flue gas of the warm process are slightly higher than in the cold removal process because less ammonia and HCN is captured.

The cost results are shown Table 7.5. Two design options are considered for the mixed WGS and CO_2 removal unit of the warm syngas cleanup process, including transport-bed reactors and multiple-stage fixed-bed reactors.

The mixed WGS and CO_2 removal unit is the most important equipment in the process, and it represents the biggest fraction of the total capital cost. The high cost of this unit results from the high CO_2 capture requirement by H_2 generation, which leads to high absorbent usage and large-size equipment, and the highly exothermic reactors, which leads to heat management challenges. Capital cost analysis results demonstrated that the total installed cost for the warm syngas cleanup process with transport-bed reactors is ~58% higher than the cold syngas cleanup process because of the high mixed WGS and CO_2 removal unit costs. The process with the fixed-bed design has a similar capital cost as the cold syngas cleanup process. The capital cost of the sulfuric acid plant in the warm gas cleanup process is higher than the sulfur plant of the cold syngas cleanup process. The warm gas cleanup process also has a higher steam turbine cost because of higher heat recovery requirement and thus higher power generation.

Table 7.4. Performance Results

	Cold Gas Cleanup	Warm Gas Cleanup
Feed	Coal syngas	Coal syngas
Flow rate, lb/h	905,267	905,267
Product	Hydrogen	Hydrogen
Flow rate, lb/h	63,693	65,953
Flow rate, MMscf/d	288	298
Byproduct	Sulfur	Sulfuric acid (98.5 wt%)
lb/h	1,658	5,145
Power summary		
Electricity generation		
Steam turbine, MW	46.07	100.81
Auxiliary load		
Particulate removal	0.47	0
WGS and AGR	15.41	1.43
Sulfur/sulfuric acid plant	1.24	0.002
Steam cycle	4.71	4.22
Circulating water pump	2.09	1.83
Cooling tower fan	0.95	0.83
Miscellaneous balance of plant	2.49	0.83
Total auxiliary load, MW	27.35	9.14
Net electricity, MW	18.72	91.67
Raw water withdrawal		
Cooling-water makeup, gpm	1879	1646
Boiler feed-water makeup, gpm	347	588
Environmental performance		
Wastewater discharge, gpm	522	643
Spent ZnO disposal, tpd	0.138	0.285
Spent trace metal adsorbent disposal, lb/d	90.3	1,722
Captured CO_2, lb/h	806,862	828,216
CO_2 emission in flue gas, lb/h	136,217	118,496
SO_2 emission in flue gas, lb/h	0	0
NOx emission in flue gas, lb/h	1,500	1,601
Energy efficiency		
Raw syngas, MMBtu/h	4,917	4,917
Net electricity, MMBtu/h	63.9	312.8
Hydrogen, MMBtu/h	3888.5	4,026
Overall energy efficiency, %	**80.39%**	**88.26%**

Table 7.5. Cost Results

2011 U.S. Dollars	Cold Gas Cleanup	Warm Gas Cleanup (Transport-Bed)	Warm Gas Cleanup (Fixed-Bed)
Capital costs, $ million			
PM and other impurities removal	11.04	11.75	11.75
PM removal	11.04	10.19	10.19
Chloride removal	Included in PM removal	1.56	1.56
Shift and AGR	**142.8**	**265.6**	**113.6**
Shift reaction only (Cold) or mixed shift and CO_2 removal (Warm)	12.8	232.8	80.8
Sulfur and CO_2 removal (Cold) or sulfur removal only (Warm)	127.4	31.52	31.52
Sulfur polish	2.60	1.24	1.24
Sulfur recovery	10.81	18.71	18.71
Trace metal	2.25	1.85	1.85
H_2 purification	47.22	48.71	48.71
Steam turbine	28.29	40.07	40.07
Balance of plant	18.96	27.00	27.00
Total installed cost (TIC), $million	**261.3**	**413.7**	**261.7**
Total indirect cost, $million	**86.25**	**136.52**	**86.35**
Total capital investment (TCI), $ million	**365.0**	**577.7**	**365.4**
Annualized TCI, $ million/yr (20 year plant life)	**18.25**	**28.89**	**18.27**
Variable operating cost, $ million/yr	**−7.42**	**−11.19**	**18.89**
Water treatment chemical	1.54	1.61	1.61
Trace metal removal	0.04	19.80	19.80
Sour shift catalyst (cold) or mixed WGS catalyst and CO_2 absorbent (warm)	0.62	12.89	42.97
Selexol solution for S and CO_2 removal (cold) or ZnO for sulfur bulk removal only (warm)	0.38	0.29	0.29
Sulfur polish ZnO absorbent	0.67	1.38	1.38
Sulfur plant catalyst	0.01	n/a	n/a
Chloride removal catalyst	n/a	4.44	4.44
Waste disposal	0.0009	1.14	1.14
Byproduct credit	−1.31	−1.66	−1.66
Electricity and other utilities	−9.36	−51.08	−51.08
Fixed operating cost, $ million/yr	18.73	18.70	18.70
Total operating cost, $ million/yr	11.31	7.51	37.59
Total annual costs, $ million/yr	**29.56**	**36.40**	**55.86**
Aggregate cost of production, $/MMscf H_2	**313**	**372**	**571**

For the transport-bed reactors, eight parallel reactors, each with an online reactor and internal cooling by steam generation and a regenerator, are assumed for the process. For the multiple-stage, fixed-bed reactor design, three-stage reactors with interstage cooling were chosen to guarantee the temperature increase for each stage to be <200°F, and a spare stage is assumed to be used offline for regeneration. Using transport-bed reactors leads to much higher capital cost because the reactor size is much larger than the reactor in a fixed-bed design to allow enough space for fluidization. This design is better for heat management and has better syngas and absorbent mixing, but its maintenance costs are higher compared to the fixed-bed design. However, using this design reduces the catalyst cost when compared to the fixed-bed reactor design. Catalyst/absorbent usage then is decided by the CO_2 uptake capacity limit, the CO_2 capture requirement per unit of time, and the regeneration time. The regeneration time is assumed to be

0.5 hour. To avoid breakthrough of the online bed, the online time for a transport-bed reactor should be at least 0.8 hour assuming a breakthrough point of 70% of the maximum capacity. For the fixed-bed design with three stages online and one stage offline, a single operating cycle needs at least 1.5 hours to ensure that every online reactor can be regenerated in series in the cycle. Therefore, for the fixed-bed reactor system, the total absorbent usage is for 2 hours of CO_2 absorption (three online units each operating for 0.5 hour plus the offline unit operating for 0.5 hour). Compared to catalyst usage of the transport-bed reactor (i.e., 0.8 hour for CO_2 absorption), catalyst usage for the fixed-bed reactor system is much higher. Therefore, the operating cost of the transport-bed process is much lower than the operating costs for the fixed-bed design. The total variable operating cost of the transport-bed design is also less than that of the cold gas cleanup process because of much higher credit from net power generation.

The overall effect is that the warm syngas cleanup process with the transport-bed design has about 19% higher aggregate cost than the cold syngas cleanup process because of the high capital cost. The fixed-bed reactor design has about 82% higher aggregate cost than the cold syngas cleanup process because of the high mixed WGS and CO_2 absorbent cost. Comparing the transport-bed design and the fixed-bed design, the transport-bed design has much lower aggregate cost because of the much lower mixed WGS and CO_2 absorbent cost. Therefore, reducing the variable cost for the mixed WGS and CO_2 absorbent is a key factor to achieving low production cost for the process investigated in this study.

To reduce the catalyst cost of the warm syngas cleanup process, the catalyst life for the mixed WGS catalyst and CO_2 absorbent must be increased. The current catalyst life of 2 years is much shorter than the 10 year catalyst life of the Selexol solution. Increasing the space velocity of the mixed WGS and CO_2 removal process has little effect on reducing catalyst/absorbent usage because absorbent usage must guarantee enough online time, which is constrained by the CO_2 uptake capacity limit of the absorbent and the required CO_2 capture flow rate. Even if higher space velocity were achieved, catalyst/absorbent usage still would be high because enough absorbent would be needed to guarantee completion of regeneration. An effective method for reducing the mixed WGS and CO_2 absorbent cost is to increase the catalyst life, thus reducing the cost for replacing spent absorbent. Figure 7.2 shows the results of the sensitivity analysis of various mixed WGS catalyst and CO_2 absorbent lives on the aggregate cost for H_2 generation. When the catalyst life increases from the original 2 years to 4 years, the mixed WGS and CO_2 removal process operation cost will decrease 50% from the original cost, and the aggregate cost of the warm syngas cleanup with the transport-bed design would be less than the aggregate cost of the cold syngas cleanup process. When the catalyst life increased to more than 6 years, the aggregate cost of both the transport-bed and fixed-bed designs is less than that of the cold syngas cleanup process. In addition, with a catalyst life of more than 6 years, the fixed-bed design begins to show cost advantages over the transport-bed design.

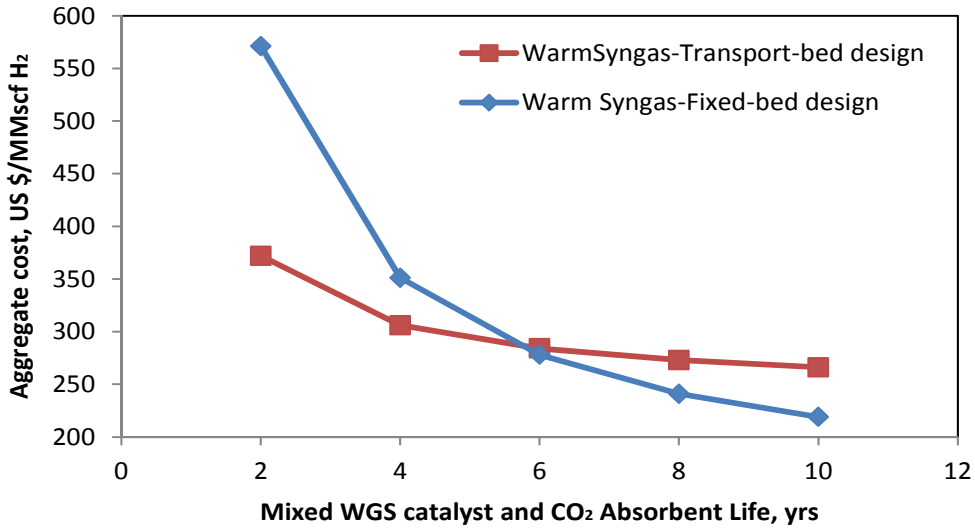

Figure 7.2. Effects of Mixed WGS Catalyst and CO2 Absorbent Life on the Aggregate Cost of Hydrogen Production

7.6 Conclusions

The major findings of this technoeconomic study are summarized below:

1. The warm syngas cleanup process reduced heat loss by dry and hot temperature operation compared to the significant heat loss associated with water quenching and scrubbing in the cold syngas cleanup process.
2. The dry and high-temperature operation of the warm syngas cleanup process leads to higher heat recovery and thus higher power generation compared to the cold syngas cleanup process.
3. The aggregate cost of warm syngas cleanup using the transport-bed design for the mixed WGS and CO_2 removal unit is lower than that of the fixed-bed design. Both of these designs cost more than of the cold syngas cleanup process because of the higher capital cost for the transport-bed reactors and higher catalyst cost for the fixed-bed reactors.
4. The warm syngas cleanup process using the transport-bed design uses less mixed WGS catalyst and CO_2 adsorbent than the fixed-bed design because the fixed-bed design needs more absorbent for longer online operating times. However, although transport-bed reactors have a short online operating time and therefore use less catalyst, the short online time and high CO_2 capture requirement lead to high absorbent circulating rate between the reactor and the regenerator, which imposes challenges on operation and maintenance of the transport-bed unit.
5. Increasing catalyst life would be an important approach to reducing the mixed WGS and CO_2 absorbent cost. Based on this work, when the catalyst life increases to more than 6 years, the fixed-bed design has a cost advantage than the transport-bed design.

6. The primary reason for the high equipment cost for the transport-bed design and high catalyst cost for the fixed-bed design is the high CO_2 capture requirement for H_2 generation. Therefore, for a system with a lower CO_2 capture requirement, such as to produce syngas for methanol synthesis, the cost disadvantages for using the CO_2 absorbent should be less than that shown in this study. The cost difference between the warm and cold syngas cleanup processes would be smaller, or the cost of warm syngas cleanup process could be lower than that of the cold syngas cleanup process.

8.0 Conclusions

In this study, we focused on developing a CO_2 capture material suitable for operating in a warm temperature range. Our primary goal was to minimize or replace the $NaNO_3$ molten salt with other melting salts that are less corrosive and, therefore, would be more amenable to integration with catalysts required for synthesis (e.g., methanation catalysts). We have found that a mixture of carbonate salts, including lithium, sodium, and potassium carbonates, are able to function analogously to $NaNO_3$ in removing CO_2 at temperatures at ~380°C or lower, and they lack the corrosiveness of the nitrate salt. Thus, we have been able to capture CO_2 at temperatures below the measured melting point of this mixture of carbonates and under conditions and temperatures that we define as "pre-melting." Although CO_2 capture capacity is not quite as high as with the nitrate salt, we moved forward with these carbonate materials in fixed-bed tests. This type of sorbent was utilized in a process demonstration.

This sorbent material was integrated with methanation catalyst to drive the equilibrium-driven methanation reaction while simultaneously providing CO_2 capture. Process conditions were optimized to match sorption-enhanced CO methanation reaction kinetics with CO_2 sorption-desorption. A single unit operation that could yield 99% conversion to CH_4 when operating at pressurized conditions (10 bar) and simultaneously capturing CO_2 was demonstrated.

Na_2CO_3 was shown to be effective for removing HCl in the presence of syngas and optimal when operated at approximately 450°C. A sorbent comprising of Cu and Ni active components was shown to be effective for the removal of a multitude of contaminants, including as AsH_3 and PH_3. Trace amount of sulfur can also be removed using this material.

A sulfur gas removal sorbent system also was developed. In particular, we focused on understanding the effects of H_2S levels, temperature, presence of COS, and cycling performance of the ZnO bed. Removal of H_2S was evaluated at ZnO bed operating temperatures of 300, 450, and 550ºC. An optimum sulfur uptake was determined when operating at 450ºC; however, the sulfur slip is thermodynamically expected to be lower at lower operating temperatures (albeit below our analytical detection limits). We also evaluated ZnO stability after multiple regeneration cycles. We found that sulfur capacity decreased after the first two cycles but remained relatively constant after three cycles. These cycling experiments showed promise for the long-term applicability for sulfur removal in a multi-cycle sorption/desorption system. A sulfur removal process using a regenerable ZnO bed operated at 450ºC while a polishing sulfur removal bed operated at 300ºC was developed. In addition to sulfur removal, additional sorbents are added to the process for complete contaminant removal.

Proof-of-concept of the integrated cleanup process was demonstrated with gasifier-generated syngas produced at the Western Research Institute using Wyoming Decker coal. When operating with a 1 SLPM feed, multiple inorganic contaminant removal sorbents and a tar-reforming bed were able to remove the vast majority of contaminants from the raw syngas. A proof-of-concept cleanup demonstration was verified through the continuous operation of a poison-sensitive copper-based WGS catalyst located downstream from the cleanup steps. Only very minimal deactivation in the WGS catalytic activity was observed, likely because of the part-per-million levels of sulfur observed on the front end of the catalyst bed. However, the vast majority of contaminates from the raw syngas were removed, thus providing proof-of-concept and viability of this warm cleanup system.

Nonetheless, there are still many areas for improvement of this process and the materials used in this study. Technoeconomic analysis indicated areas of improvement are still needed for successful future implementation. For example, further developing the CO_2 sorbent to increase kinetics is critically needed. Relatively high equipment costs for the integrated synthesis and sorption bed(s) would be alleviated for systems with lower CO_2 capture requirements, such as to produce syngas instead of natural gas or hydrogen. In addition, there still are small levels of sulfur slipping through the warm cleanup sorbent materials, and this issue needs to be addressed before successful long-term operation can be implemented. Finally, many of the inorganic contaminants other than sulfur need to be addressed. Some of the contaminants present in real syngas probably would have been removed in the water wash prior to syngas bottling. In a real application of warm cleanup, water washing would not occur. Mercury removal and the removal of other impurities present in coal need to be further evaluated. However, successful demonstration for the proof-of-concept—particularly for regenerable sulfur removal and warm CO_2 capture—was very encouraging.

9.0 References

Black J. 2010. *Cost and Performance Baseline for Fossil Energy Plants. Volume 1: Bituminous Coal and Natural Gas to Electricity*. DOE/NETL-2010/1397, Revision 2, Morgantown, West Virginia.

Cayan FN, M Zhi, SR Pakalapati, I Celik, N Wu, and R Gemmen. 2008. "Effects of Coal Syngas Impurities on Anodes of Solid Oxide Fuel Cells." *Journal of Power Sources* 185(2):595–602.

Couling DJ. 2012. "Evaluation of Sorbents for the Cleanup of Coal-Derived Synthesis Gas." Massachusetts Institute of Technology, Cambridge, Massachusetts.

Craig KR and Mann MK. 1996. *Cost and Performance Analysis of Biomass-Based Integrated Gasification Combined-Cycle (BIGCC) Power Systems*. NREL/TP-430-21657, National Renewable Energy Laboratory, Golden, Colorado.

Davidson JM, PJ Denny, CH Lawrie, and CH Lawriea. 1989. "Autocatalysis by Water in the Reaction of Hydrogen Sulphide with Zinc Oxide." *Chemical Communications* 21(1989):1695–1696.

Davidson J and K Sohail. 1995. "A DRIFTS Study of the Surface and Bulk Reactions of Hydrogen Sulfide with High Surface Area Zinc Oxide." *Industrial and Engineering Chemistry Research* 34(1995):3675–3677.

Efthimiadis EA and SV Sotirchos. 1993. "Effects of Pore Structure on the Performance of Coal Gas Desulfurization Sorbents." *Chemical Engineering Science* 48(11):1971–1984.

Elseviers WF and H Verelst. 1999. "Transition Metal Oxides for Hot Gas Desulphurisation." *Fuel* 78:601–612.

Graedel TE, GW Kammlott, and JP Franey. 1981. "Carbonyl Sulfide: Potential Agent of Atmospheric Sulfur Corrosion." *Science* 80(212):663–665.

Gupta RP, BS Turk, and DC Cicero. 2001. "Desulfurization of syngas in a transport reactor," *Environmental Progress and Sustainable Energy* 20(3):187–195.

Howard CJ, RA Dagle, VM Lebarbier, JE Rainbolt, L Li, and DL King. 2013. "Progress toward Biomass and Coal-Derived Syngas Warm Cleanup: Proof-of-Concept Process Demonstration of Multicontaminant Removal for Biomass Application." *Industrial and Engineering Chemistry Research* 52(2013):8125–8138.

King DL and L Li. 2011. "Integrated System for Cleanup of Warm Syngas Produced from Coal or Biomass Gasification." American Chemical Society Conference Presentation, August 29, 2011, Denver, Colorado.

Kopyscinski J, TJ Schildhauer, and SMA Biollaz. 2010. "Production of Synthetic Natural Gas (SNG) from Coal and Dry Biomass – A Technology Review from 1950 to 2009." *Fuel* 89(2010):1763–1783.

Lebarbier VM, RA Dagle, L Kovarik, KO Albrecht, X-H Li, L-Y Li, CE Taylor, X-H Bao, and Y Wang. 2014. " Sorption-Enhanced Synthetic Natural Gas (SNG) Production from Syngas: A Novel Process Combining CO Methanation, Water-Gas Shift, and CO_2 Capture." *Applied Catalysis B: Environment* 144 (2014):223–232.

Lew S, K Jothimurugesan, and M Flytzani-Stephanopoulos. 1989. "High-Temperature H_2S Removal from Fuel Gases by Regenerable Zinc Oxide-Titanium Dioxide Sorbents." *Industrial and Engineering Chemistry Research* 28(1989):535–541.

Lew S, AF Sarofim, and M Flytzani-Stephanopoulos. 1992. "Sulfidation of Zinc Titanate and Zinc Oxide Solids." *Industrial and Engineering Chemistry Research* 31(8):1890–1899.

Li L and DL King. 2006. "H_2S removal with ZnO during Fuel Processing for PEM Fuel Cell Applications." *Catalysis Today* 116(4):537–541. DOI: 10.1016/j.cattod.2006.06.024.
King, J Liu, Q Huo, K Zhu., C Wang, M Gerber, D Stevens, Y Wang. 2009. "Stabilization of Metal Nanoparticles in Cubic Mesostructured Silica and its Application in Regenerable Deep Desulfuization of Warm Syngas." *Chem. Matter* 21(2009): 5358−5364.

Liu K and Q Qin. 2012. "System for Producing Methane-Rich Gas and Process for Producing Methane-Rich Gas using the Same." China.

Mei D, VM Lebarbier, R Rousseau, VA Glezakou, KO Albrecht, L Kovarik, M Flake, and RA Dagle. 2013. "Comparative Investigation of Benzene Steam Reforming over Spinel Supported Rh and Ir Catalysts." *ACS Catalysis*. 13 (2013):1133-1143.

Mei D, VA Glezakou, VM Lebarbier, L Kovarik, H Wan, KO Albrecht, R Rousseau , and RA Dagle. 2014. "Highly Active and Stable MgAl2O4-supported Rh and Ir catalysts for Methane Steam Reforming: A Combined Experimental and Theoretical Study." *Journal of Catalysis*. 316(2014): 11-23.

Meng XM, W De Jong, and AHM Verkooijen. 2009. "Thermodynamic Analysis and Kinetics Model of H_2S Sorption Using Different Sorbents." *Environmental Progress and Sustainable Energy* 28(3)360–371.

National Energy Technology Laboratory (NETL). 2000. *Texaco Gasifier IGCC Base Cases*. PED-IGCC-98-001, July 1998, Latest Revision June 2000, Morgantown, West Virginia.

Novochinskii II, C Song, X Ma, X Liu, L Shore, J Lampert, RJ Farrauto, and J Lampart. 2004. "Low-Temperature H_2S Removal from Steam-Containing Gas Mixtures with ZnO for Fuel Cell Application. 1. ZnO Particles and Extrudates." *Energy & Fuels* 18(2):576–583.

Rhodes C, SA Riddel, J West, BP Williams, and GJ Hutchings. 2000. "The Low-Temperature Hydrolysis of Carbonyl Sulfide and Carbon Disulfide: A Review." *Catalysis Today* 59(3-4):443–464.

Rosso I, C Galletti, M Bizzi, G Saracco, and V Specchia. 2003. "Zinc Oxide Sorbents for the Removal of Hydrogen Sulfide from Syngas." *Industrial and Engineering Chemistry Research* 42(8):1688–1697.

Rostrup-Nielsen J and K Pedersen. 2010. "Sulfur Poisoning of Boudouard and Methanation Reactions on Nickel Catalysts." *Journal of Catalysis* 59(1979):395–404.

Sasaoka E, S Hirano, S Kasaoka, and Y Sakata. 1994. "Characterization of Reaction between Zinc Oxide and Hydrogen Sulfide." *Energy & Fuels* 8(1994):1100–1105.

Sasaoka E. 1995. "Soot Formation over Zinc Ferrite High-Temperature Desulfurizaiton Sorbent." *Energy & Fuels* 9(1995):344–353.

Sasaoka E, K Taniguchi, MA Uddin, and S Kasaoka. 1996. "Characterization of Reaction between ZnO and COS." *Industrial and Engineering Chemistry Research* 2(1996):2389–2394.

Spath P, A Aden, T Eggeman, M Ringer, B Wallace, and J Jechura. 2005. *Biomass to Hydrogen Production Detailed Design and Economics Utilizing the Battelle Columbus Laboratory Indirectly-Heated Gasifier*. NREL/TP-510-37408, National Renewable Energy Laboratory, Golden, Colorado.

Tamhankar SS, M Bagajewicz, GR Gravalas, PK Sharma, and M Flytzani-Stephanopoulos. 1986. "Mixed-Oxide Sorbents for High-Temperature Removal of Hydrogen Sulfide." *Industrial and Engineering Chemical Process Design and Development* 25(1986):429–437.

Torres S, S Pansare, and JGJ Goodwin. 2007. "Hot Gas Removal of Tars, Ammonia, and Hydrogen Sulfide from Biomass Gasification Gas." *Catalysis Reviews: Science and Engineering* 49(4):407–456.

Verdone N and P De Filippis. 2006. "Reaction Kinetics of Hydrogen Chloride with Sodium Carbonate." *Chemical Engineering Science* 61(22):7487–7496.

Volkova LF. 1958. *Izv. Sib. Otd. Akad. Nauk SSSR* 7:33-35.

Wettlaufer JS and MG Worster. 2006. "Premelting Dynamics." *Annual Review of Fluid Mechanics* 38:427–452. DOI: 10.1146/annurev.fluid.37.061903.175758.

Winter M. 2012. "Web Elements." Available: http://www.webelements.com/.

Xiao Y, Z Li, B Wang, L Zhao, and J Chi. 2012. "Thermodynamic Performance Assessment of IGCC Power Plants with Various Syngas Cleanup Processes." *Journal of Thermal Science* 21(5):391–403.

Zhang K, XS Li, Y Duan, DL King, P Singh, and L Li. 2013. "Roles of Double Salt Formation and $NaNO_3$ in Na_2CO_3-Promoted MgO Absorbent for Intermediate Temperature CO_2 Removal." *International Journal of Greenhouse Gas Control* 12**:**351–358.

Zhang K, X-S Li, W-Z Li, A Rohatgi, Y Duan, P Singh, L Li, and DL King. 2014. "Phase Transfer-Catalyzed Fast CO_2 Absorption by MgO-Based Absorbents with High Cycling Capacity." *Advanced Material Interface*. DOI: 10.1002/admi.201400030.

Zhao J, J Huang, X Wei, Y Fang, and Y Wang. 2007. "Regeneration Characteristics of Sulfided Zinc Titanate Sorbent for Hot Gas Cleaning." *Journal of Fuel Chemistry Technology* 35(1):65–71.

Appendix A

Process Flow Diagrams for Cold and Warm Syngas Cleanup Processes

Appendix A

Process Flow Diagrams for Cold and Warm Syngas Cleanup Processes

Process flowsheets for the Cold Syngas Cleanup Process, Warm Gas Cleanup Process (Transport-Bed), and Warm Gas Cleanup Process (Fixed-Bed) are provided in this appendix.

Cold Syngas Cleanup Process

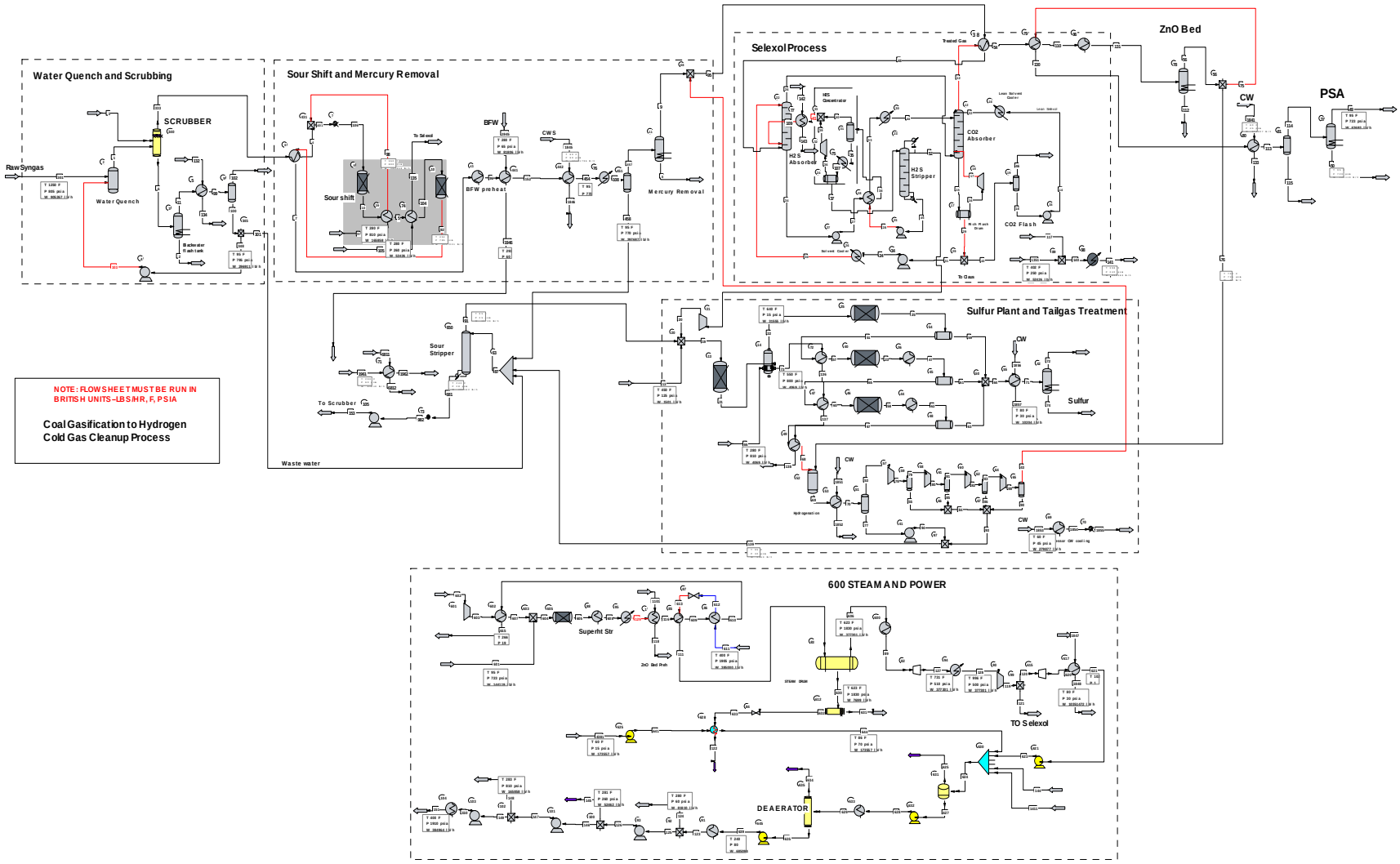

Warm Gas Cleanup Process (Transport-Bed)

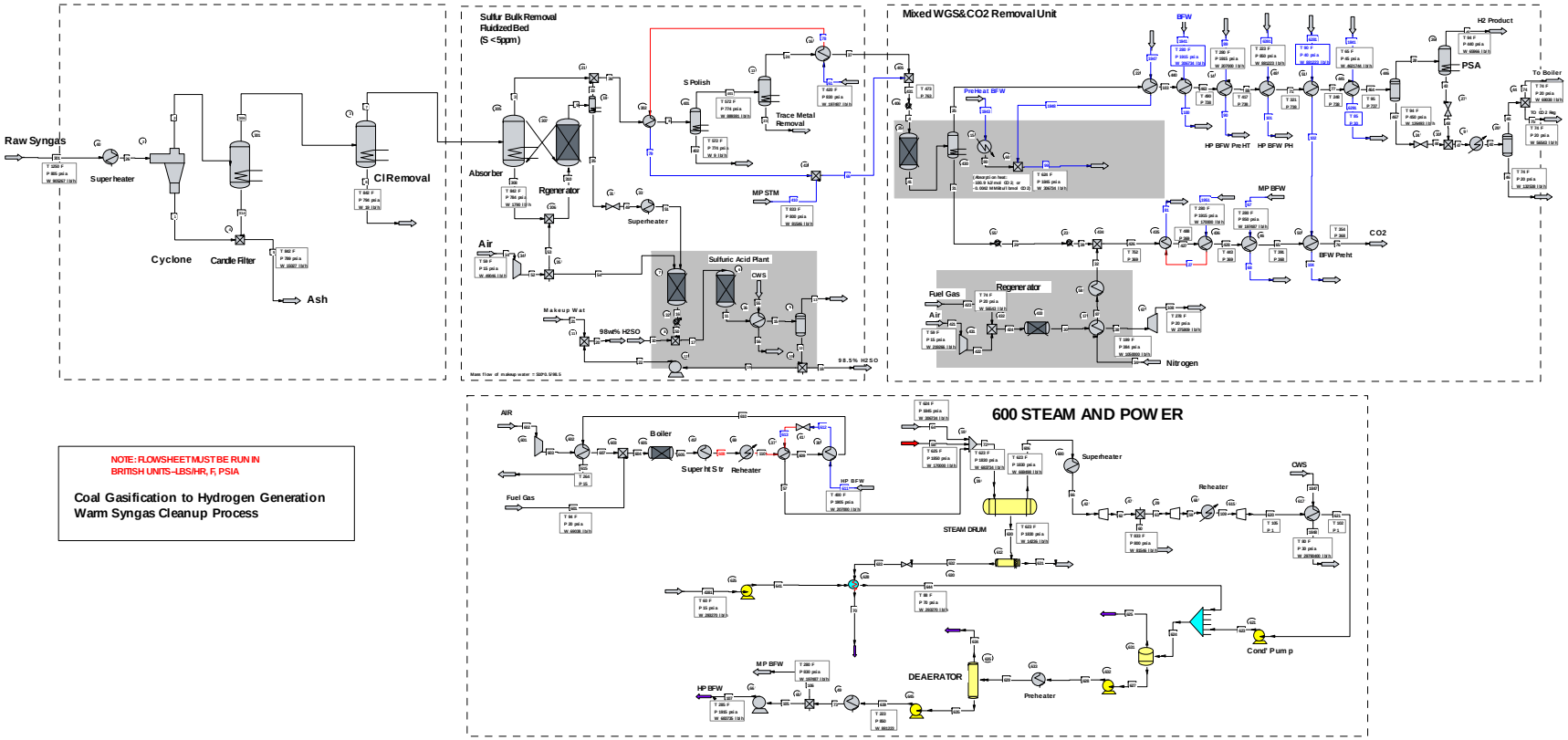

NOTE: FLOWSHEET MUST BE RUN IN BRITISH UNITS -LBS/HR, F, PSIA

Coal Gasification to Hydrogen Generation
Warm Syngas Cleanup Process

Warm Gas Cleanup Process (Fixed-Bed)

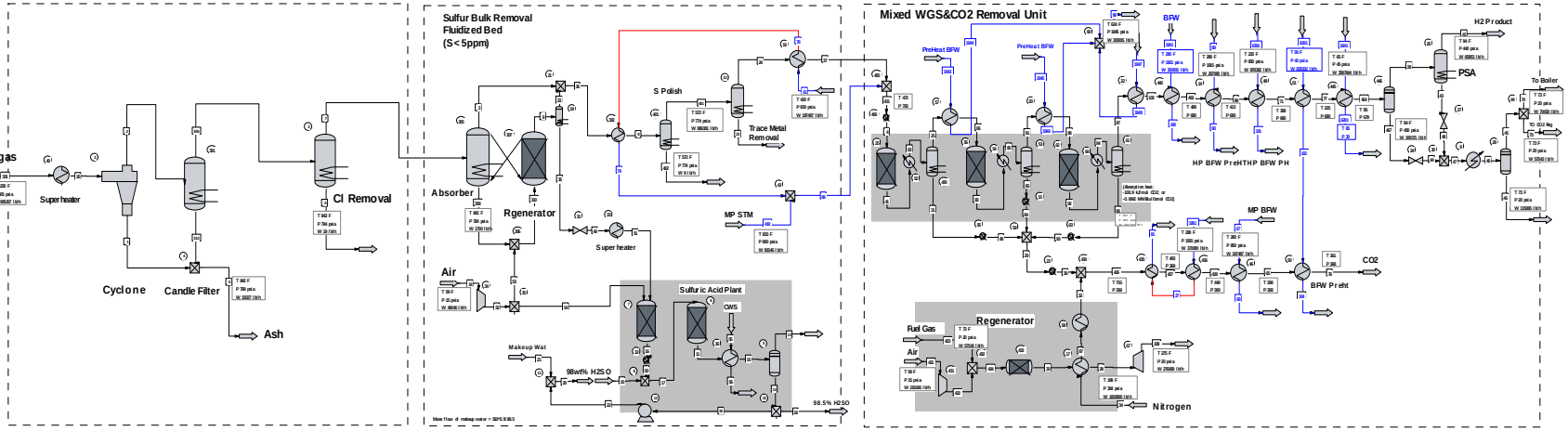

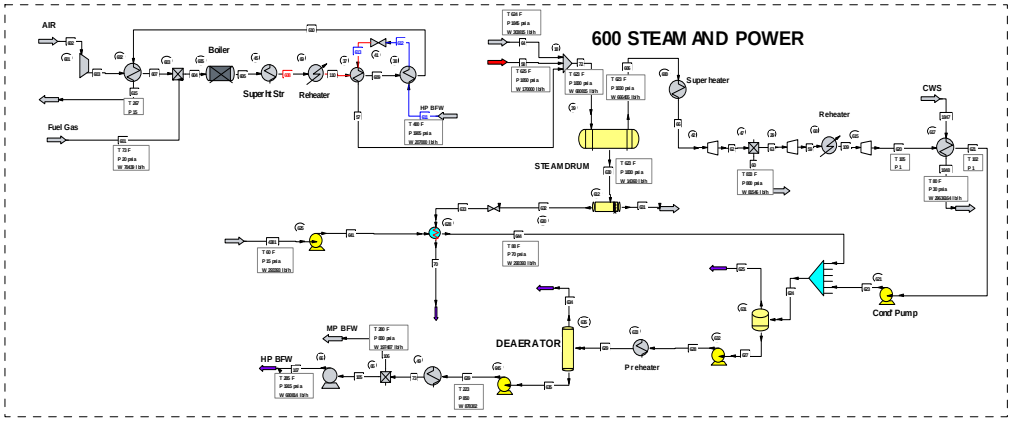

NOTE: FLOWSHEET MUST BE RUN IN BRITISH UNITS--LBS/HR, F, PSIA

Coal Gasification to Hydrogen Generation
Warm Syngas Cleanup Process

Distribution

University of Wyoming
School of Energy Resources
Dept. 3012, 1000 E. University Avenue
Laramie, WY 82071
Diana Hulme
Associate Director of Energy Research

Western Research Institute – Energy Production & Generation
3474 N. 3rd Street
Laramie, WY 82072
Beau Braunberger
Lead Engineer

Local Distribution
Pacific Northwest National Laboratory
RA Dagle
DL King
XS Li
R Ling
KA Spies
Y Zhu
JE Rainbolt
L Li
T Brouns
C Freeman

Pacific Northwest
NATIONAL LABORATORY

Proudly Operated by **Battelle** *Since 1965*

U.S. DEPARTMENT OF
ENERGY

902 Battelle Boulevard
P.O. Box 999
Richland, WA 99352
1-888-375-PNNL (7665)
www.pnnl.gov